https://doi.org/10.5194/egusphere-2025-1297
Preprint. Discussion started: 5 May 2025

UAV LiDAR surveys and machine learning improves snow depth and water equivalent estimates in the boreal landscapes

Maiju Ylönen[1], Hannu Marttila[1], Anton Kuzmin[2], Pasi Korpelainen[2], Timo Kumpula[2], Pertti Ala-Aho[1]

[1] Water, Energy and Environmental Engineering Research Unit, University of Oulu, Oulu, 90014, Finland
[2] Department of Geographical and Historical Studies, University of Eastern Finland, 80101, Joensuu, Finland

Correspondence to: Maiju Ylönen (maiju.ylonen@oulu.fi)

Abstract

Climate change is rapidly altering snow conditions worldwide and northern regions experiencing particularly significant impacts. As these regions warm faster than the global average, understanding snow distribution and its properties at both global and local scales is critical for effective water resource management and environmental protection. While satellite data and point measurements provide valuable information for snow research and models, they are often insufficient for capturing local-scale variability. To address this gap, we integrated UAV LiDAR with daily reference measurements, snow course measurements and machine learning (ML) approach. By using ML clustering, we generated high-resolution (1 m) snow depth and snow water equivalent (SWE) maps for two study areas in northern Finland. Data were collected in four different field campaigns during the 2023–2024 winter season. The results indicate that snow distribution in the study areas can be classified into three distinct categories based on land cover: forested areas, transition zones with bushes, and open areas namely peatlands, each showing different snow accumulation and ablation dynamics. Cluster-based modelled SWE values for the snow courses gave good overall accuracy, with RMSE values of 31–36 mm. Compared to snow course measurements, the cluster-based model approach enhances the spatial and temporal coverage of continuous SWE estimates, offering valuable insights into local snow patterns in the different sites. Our study highlights the influence of forests and forest gaps on snow accumulation and melt processes, emphasizing their role in shaping snow distribution patterns across different landscape types in arctic boreal zone. The results improve boreal snow monitoring and water resource management and offer new tools and high-resolution spatiotemporal data for local stakeholders working with hydrological forecasting and climate adaptation and supporting satellite-based observations.

Keywords: remote sensing, drones, snow, arctic, mapping, spatial

1 Introduction

Snow is an important part of the hydrological cycle and highly relevant for societies and ecosystems, especially in high latitude and mountainous regions. Snow cover, the timing and distribution influences directly on climate energy budget through snow albedo (Callaghan et al., 2011; Li et al., 2018), ecosystems and habitats including species and vegetation distribution (Thiebault & Young, 2020), biogeochemical processes in soils and seasonal ground frost (Ala-Aho et al., 2021; Croghan et al., 2023; Jan & Painter, 2020). Additionally, snow resources have a major impact on catchment, river and groundwater water budgets and seasonal distribution (Meriö et al., 2019). Snow-covered areas are decreasing as global temperatures rise, leading to a consistent decline in snow water equivalent (SWE**)** (Colombo et al., 2022; Faquseh & Grossi, 2024; Kunkel et al., 2016; Räisänen, 2023; Y. Zhang & Ma, 2018)**.** A recent study by Gottlieb & Mankin (2024) shows that snowpack has decreased in half of the Northern Hemisphere river basins and the declines are highly related to human actions. The timing and amount of snowmelt, along with the SWE during the melting period, are crucial for local water balance and floods (i.e., Bavay et al., 2013; Callaghan et al., 2011; Wang et al., 2016). Changes in snow conditions and rising temperatures are causing earlier flood peaks in snowmelt-dominated

https://doi.org/10.5194/egusphere-2025-1297
Preprint. Discussion started: 5 May 2025

catchments with a decline in streamflow later in the year (Berghuijs & Hale, 2025; Engelhardt et al., 2014; Matti et al., 2017). Snowmelt significantly influences near-surface hydrological effects (Muhic et al., 2023) and soil moisture in these regions (Okkonen et al., 2017).

Snow models are an important part of water resource planning and prediction. These models provide estimations of snow related hydrological parameters for areas and times where ground observations are not available and can be used for creating various scenarios. However, accurate prediction of snow-water resources, snow models require high-resolution data as input, testing and validation. Satellite based remote sensing is still rather a coarse resolution and has limited accuracy with canopy cover (Muhuri et al., 2021; Rittger et al., 2020). Thus ground-based manual measurements for feeding operational models are still conducted. The snow course network provides important data for models and serve as a long-term historical dataset; however, they are time-consuming, the accuracy varies (Beaudoin-Galaise & Jutras, 2022; Kuusisto, 1984; Mustonen, 1965), and temporal resolution is weeks to month. Thus, it is not ideal for capturing peak snow depth or melt-out dates (Malek et al., 2020).

To bridge the knowledge and technical gap between remote and ground observations, uncrewed aerial vehicles (UAV) have been proven to be efficient in the snow depth and SWE estimations with decent cost and accuracy (e.g., (Adams et al., 2018; Niedzielski et al., 2018; Rauhala et al., 2023). Like satellite platforms, also UAV systems can carry both optical and radar-based sensors and provide high resolution spatial information. Photogrammetry, including RGB and stereo-imagery, can result in centimeter-scale accuracy in snow depth mapping over catchment scale and has relatively low cost compared to radars like ground-penetrating radar (GPR) and light detection and ranging (LiDAR) (Maier et al., 2022; Nolan et al., 2015; Rauhala et al., 2023). However, photogrammetry-based products, like structure-from-motion (SfM), have limitations in lighting conditions and dense vegetation, and the decision between cost-effectiveness and accuracy is dependent on the site characteristics (Rauhala et al., 2023; Rogers et al., 2020). Recently LiDAR sensors have got more affordable, compact and lightweight. Technical advancements, such as improved inertial measurement unit (IMUs) and global navigation satellite systems (GNSS), have enhanced their accuracy and performance, making LiDAR more cost-effective and competitive compared to UAV photogrammetry (Bhardwaj et al., 2016; Rogers et al., 2020). The UAV LiDAR technology potentially offers high accuracy over large spatial areas and allows catchment-scale mapping also even under canopy cover, unaffected by overcast conditions or shadows (Dharmadasa et al., 2022; Harder et al., 2020; Jacobs et al., 2021; Mazzotti et al., 2019). LiDAR based snow depth data can also be used to estimate the spatial distribution of SWE in landscape scale in a decent cost-effectiveness (Broxton et al., 2019; Geissler et al., 2023).

Snow conditions are mostly controlled by temperature and precipitation (Mudryk et al., 2020; Mudryk et al., 2017), and changes in global and local climate trends impact snow cover differently across regions. However, local snow accumulation is dependent on-site characteristics, such as topography, vegetation, and weather and wind distribution (Currier & Lundquist, 2018; Mazzotti et al., 2019, 2023). Forest structure significantly affects snow accumulation (Mazzotti et al., 2023) and SWE values for forested areas appear significantly higher than in tundra and shrub tundra zones (Busseau et al., 2017; Dharmadasa et al., 2023). The effect of forest structure to snow melt also depends on the climate, as in cold regions, snow lasts longer in forests than in forest openings, whereas in warm climates, it stays longer in forest clearings (Lundquist et al., 2013). Additionally, snowpack characteristics are spatially different in forest gaps (Bouchard et al., 2022) and edges (Currier et al., 2022; Mazzotti et al., 2019). Vegetation changes, such as the northward retreat of the tree line, densification of existing vegetation and migration of new species towards the poles, will also affect snow dynamics and its effects are not yet fully known (Aakala et al., 2014; Franke et al., 2017; Grace et al., 2002; Ropars & Boudreau, 2012). For better understanding of snow processes, we need improved tools and approaches, especially with localized high resolution spatial data.

Even though annual changes in snow cover are dominated by the weather conditions, different patterns, “clusters”, of snow distribution and melting can be detected (Currier et al., 2022; Geissler et al., 2023; Matiu et al., 2021). These snow distribution clusters are site-specific and dictated by the local site characteristics, and importantly they can be

https://doi.org/10.5194/egusphere-2025-1297
Preprint. Discussion started: 5 May 2025

extended to different years (Pflug & Lundquist, 2020; Sturm & Wagner, 2010). Revuelto et al. (2020) successfully modeled daily snow depth maps using in-situ measurements and time-lapse photographs, and collected field data from two winters was estimated to be enough for the random forest model to estimate snow depth for other years. Repetitive UAV surveys over the winter season can similarly provide spatial information of snow cover, helping to identify factors affecting snow distribution. Different machine learning approaches have shown promising results in snow depth and SWE mapping for different regions (J. Zhang et al., 2021), as they can reduce biases and enhance overall accuracy (King et al., 2020; Vafakhah et al., 2022), but uncertainties and challenges call for more testing in different conditions (Meloche et al., 2022; Revuelto et al., 2020). Especially, the accurate definition of SWE from snow depth clusters still presents challenges (Geissler et al., 2023).

Our study produces spatial daily snow depth and SWE estimates in different sites based on a combination of LiDAR-based snow depth maps, snow course measurements and continuous snow depth measurements. The field data was collected during winter 2023-24 from two different sites in the Finnish Lapland, each with long-term monitoring infrastructure and existing snow course measurements, representing different vegetational and topographical conditions typical for the boreal and sub-arctic landscapes. In this study, we investigate the ability of UAV LiDAR method to map snow depth in forested boreal and sub-arctic sites across northern Finland. We discuss how snow-depth clusters and characteristics derived from machine learning could be used to improve SWE estimates in our study sites in substantially higher spatial and temporal resolution compared to traditional operational snow course measurements. We also evaluate the output of the LiDAR-based snow clustering and model SWE estimates and compare them to the snow course measurements in each site.

2 Data and methods

2.1 Study areas

Three study areas were chosen to present different environmental conditions of the Finnish Lapland and sub-arctic and boreal zone, namely Pallas (Fig. 1a), Sodankylä (Fig. 1b). All sites have on-going snow course measurements operated by the Finnish Environment Institute (SYKE), at least one ultrasonic snow depth sensor together with weather station operated by the Finnish Meteorological institute (FMI) and all data is open access (Sect. 2.2.4).

Pallas (67° 59’ N, 24° 14’ E) is the northernmost among the study sites and located the highest from the sea level. The land cover is mostly coniferous forests (63%), with mires and mixed forests (Table 1). Pallas mean total annual precipitation is 644 mm, and mean wintertime precipitation of 233 mm, mean annual temperature 0.5 °C and mean wintertime temperature -7.0 °C. It has an average of the highest snow depths compared to the other sites. Sodankylä is located the middle part of Lapland (67° 21' N, 26° 37' E), the land cover is mainly mire (63%) and the elevation range is low (Table 1). Sodankylä site is in the FMI research station, which has daily weather observations since 1908 (The Finnish meteorological institute, 2025). Sodankylä mean total annual precipitation is 553 mm, and mean wintertime 202 mm, mean annual temperature 0.9 °C and mean wintertime temperature -7.6 °C.

Table 1. Meteorological and landscape characteristics for Pallas and Sodankylä.

	Pallas	Sodankylä	Data source
Elevation range. m	267-350	178-183	NLS
Mean annual air temperature (°C) 2008-2024	0.5	0.9	FMI
Mean annual total precipitation (mm) 2008-2024	644	553	FMI
Average snow depth Nov-May (cm) 2008-2024	65	48	FMI
Average winter wind direction Nov-Apr (°)	199	182	FMI

https://doi.org/10.5194/egusphere-2025-1297
Preprint. Discussion started: 5 May 2025

Lidar extent (km²)	0.8	1.1	
Land cover (%): *deciduous*	0.1	0.1	SYKE Corine land cover 2018
coniferous	62.7	27.0	
mixed	14.9	3.7	
mire	17.2	62.7	
canopy closure <30 %	3.5	4.1	

Data sources: *FMI (2025), SYKE (2018), National Land Survey of Finland (NLS) (2020).*

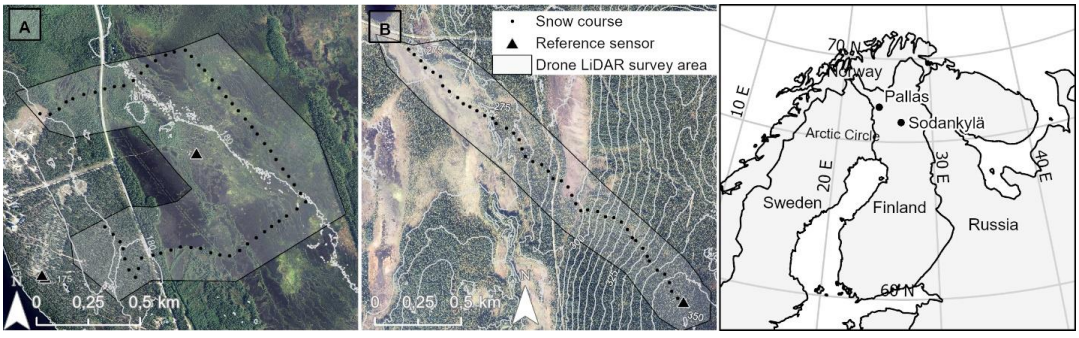

135 **Figure 1. Location and maps of study sites (a) Sodankylä (b) Pallas. Gray area represents UAV-flight areas and black points manual snow sampling locations and snow courses. Orthophoto from the National Land Survey of Finland.**

2.2 Field measurements

In our field campaigns, four snow-on and one snow-off LiDAR surveys were conducted in both sites during the winter of 2023-2024. The aim was to capture the snowpack in its different stages of winter: i) new snowpack, ii) maximum
140 snowpack, and iii) late, melting snowpack, to distinguish areas in each site with similar snow patterns and variability (Fig. 2). Winter 2023-2024 the snow depths were above the average in Pallas and Sodankylä. In both sites, snow depth started to decrease in March 2024, but increased again later in April 2024 due to heavy snowfall events (Fig. S3, supplementary materials).

https://doi.org/10.5194/egusphere-2025-1297
Preprint. Discussion started: 5 May 2025

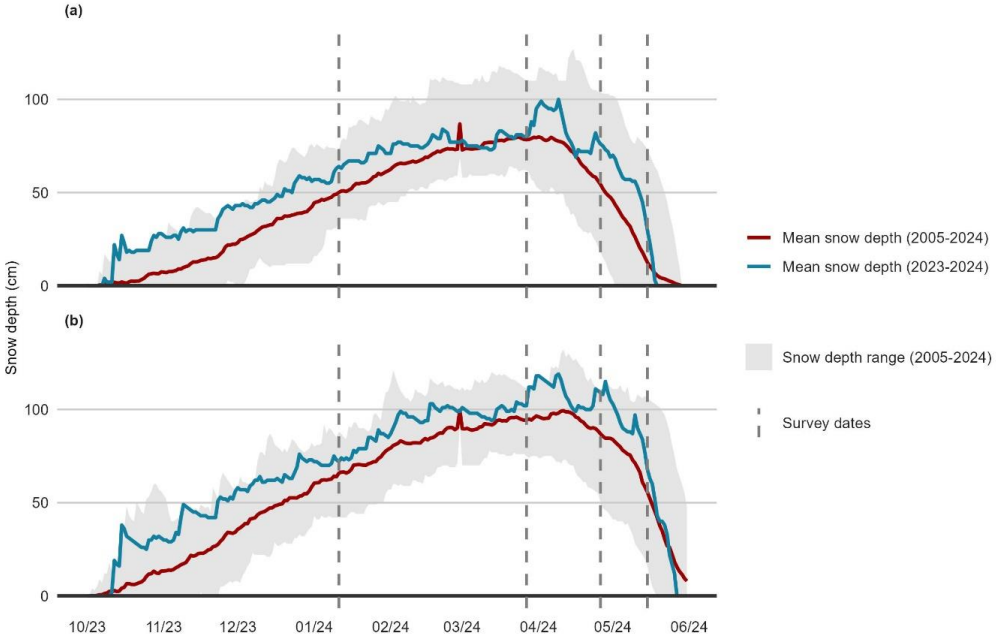

Figure 2. Snow depts from each site's FMI stations. Sodankylä (a), Pallas (b). Dark dashed lines represent the UAV drone campaign dates from the winter 2023-2024.

2.2.1 UAV LiDAR surveys

UAV LiDAR mapping was performed at Sodankylä and Pallas using YellowScan Mapper+ (YellowScan, France), equipped with an Applanix APX-15 inertial measurement unit and mounted on a DJI Matrice 300 RTK (DJI, Shenzhen, China). The scanner operated with a 70.4° scanning angle and a 240 kHz pulse repetition frequency, with both sites scanned at a cruising speed of 7 m/s, an altitude of 80 m above ground level, and a 70% overlap between flight lines (Table S1. appendices). Trajectory correction was made in Applanix POSPac software using continuously operating reference station (CORS) observations from National Land Survey of Finland CORS network as the reference data.

We compared the accuracy of the DTMs between different data processing methods, using 5 GCP (ground control point) as a reference. We tested Cloudstation's MinZ and Meanz methods and compared the lasR (v4.1.2; Roussel et al., 2020) and lidR packages (v0.13.0; Roussel, 2024) in R for DTM calculation. The models from the Cloudstation MinZ method best matched the accuracy of the 5 GCP plates and we chose the models produced by this method. However, it should be noted that the DTMs of May campaign in Sodankylä produced by Cloudstation have notably poorer accuracy compared to the DTMs produced by other methods. However, as the other campaign DTMs were the most accurate, we decided to use the same method for each site and campaign and accept the May inaccuracies. In addition, for each campaign, the data shows a DTM upscaling along the trajectory line borders, approx. 1-5 cm. The uplifts are presumably due to poorer georeferencing of points at the trajectory edges and presumably overlapping points from the two trajectories cause abnormal surfaces in DTMs. We tried to clean up the data from overlapping points, but the overall accuracy of the DTM was degraded, so we chose to accept the inaccuracies in the UAV flight trajectory edge regions.

https://doi.org/10.5194/egusphere-2025-1297
Preprint. Discussion started: 5 May 2025

2.2.3 Manual snow measurements

Manual snow depth and density measurements were conducted on the same day as the UAV LiDAR flights and used as verification and validation data for modelled maps. Within 6 hours of each survey, snow course measurements were done through the study areas following the SYKE snow survey protocol (Kuusisto, 1984; Mustonen, 1965). Snow depth was measured every 50 m and density every 200 m along the snow course transect in Pallas (Fig. 1a). In Sodankylä, where the snow course is longer (4 km) the SWE was measured in 8 different sites along the snow course representing different terrain types (Fig. 1b). Snow measurements points were geolocated using RTK GPS Emlid RS2+ (Hungary) and Trimble GNSS system R12i (USA).

2.2.4 Automatic daily snow depth measurements

At least one snow depth sensor (Campbell Scientific SR50) can be found from each of the study sites. In Sodankylä, the study site is equipped with three daily snow depth ultrasonic sensors across different environments to capture the variability in snow cover (Fig. 1b). The sensors are operated by FMI and data is open access (https://litdb.fmi.fi/index.php). Sensors are in open peatland (N67°22.024', E26°39.070'), pine forest opening (N67°21.706', E26°38.031') and inside sparse pine forest (N67°21.699', E26°38.051'). Pallas has one daily snow depth ultrasonic sensor located in Kenttärova (Fig. 1a) also operated by FMI (https://en.ilmatieteenlaitos.fi/download-observations). The sensor is in the spruce forest in the upper part of the study area (N67°59.237', E24°14.579').

2.3 Data analysis

2.3.1 LiDAR data processing

LiDAR data from each campaign were pre-processed using CloudStation software. As part of this process, we performed strip alignment of the flight lines to generate an accurately georeferenced point cloud. To classify points belonging to the ground, we applied the following parameters: steepness (which reflects terrain variation) was set to 0.2, minimum object height (the vertical threshold above which an object is not considered part of the ground) was set to 0.03 m, and point cloud thickness was set to 0.15 m. Following classification, we generated two types of DTMs: MinZ and MeanZ, where the Z value represents the minimum and mean elevation, respectively, for each pixel. Both DTMs were produced with a 10 cm spatial resolution. MinZ DTM showed better correspondence with the GCP plates (Sect. 2.2.1) and was used in the following analysis.

Further DTM processing was conducted using ArcGis Pro 3.2.0. The snow depth rasters were generated by calculating the difference between two DTMs: one collected during the winter season and the other from a bare ground survey at the end of May/beginning of June. To standardize spatial resolution, the snow depth rasters were then resampled to 1m resolution. Snow depth values falling outside a reasonable range (<-0,5m; > 2m) were set to null to remove extreme outliers, while minor negative values close to zero were corrected to zero (-0,5 – 0). Missing values were filled by calculating the median value from surrounding cells, using the neighborhood median of 5x5 cell grid. The data was clipped to area of interest (AOI), focusing the analysis on the buffer zone of 150m around the snow courses.

The error metrics were calculated using the 5 ground control points around the study areas and comparing their accuracy to the derived DTMs following the suggestion of Rauhala et al. (2023). To estimate the uncertainty of generated DTMs, the difference between UAS DTMs and RTK measured GCP elevation (Δz) was calculated following Equation 1:

$$\Delta z_t = DSMs_t - z_{GCP}t, \qquad \text{(Eq 1)}$$

https://doi.org/10.5194/egusphere-2025-1297
Preprint. Discussion started: 5 May 2025

where t is the date of survey, DTM_S is the snow surface elevation from the UAS survey, and z_{GCP} is the GCP elevation measured with RTK.

When the snow depth rasters are derived from two DTMs, their precision was estimated following Equation 2:

$$\boldsymbol{u} = \sqrt{\sigma(\Delta z_t)^2 + \sigma(\Delta z_G)^2}, \quad \text{(Eq 2)}$$

where $\sigma(\Delta z_t)$ is the standard deviation for the difference between UAS DTM and RTK measured GCP elevation Δz for every winter campaign and $\sigma(\Delta z_G)$ is the standard deviation for the difference between UAS DTM and RTK measured GCP elevation Δz for bare-ground campaign.

To estimate the trueness of the calculated snow depth rasters, error propagation for mean error of snow-on and bare-ground DTMs was calculated. It is calculated by finding the average of the differences between the UAS DTMs and the GCP elevations, following Equation 3:

$$\boldsymbol{m} = \mu(\Delta z_t) - \mu(\Delta z_G), \quad \text{(Eq 3)}$$

where $\mu(\Delta z_t)$ is the mean error for the difference between each snow-on campaign DTMs and GCPs, and $\mu(\Delta z_G)$ is the mean error for the difference between bare-ground campaign DTMs and GCPs.

2.3.2 Clustering of snow lidar data sets

All analyses were performed using R Statistical Software (v.4.3.0, R Core Team, 2023). We used K-means clustering (Hartigan & Wong, 1979) to classify snow depth clusters for each study area. Clusters were identified from a smaller, random sample of the data. The detected clusters serve as a basis for the following random forest classification, which determines the clusters for the remaining study area. The classification results in a collection of two layers, first describing the probability (w) of each cell (ij) belonging to a specific cluster (c) w_{ij} and the other one describing which cluster the cell is the most likely to be associated with. Choosing the optimal number of clusters is a central step in K-means clustering, and various indices can be used to guide this decision, and we analyzed the indices with the NbClust R package (v3.0.1; Charrad et al., 2014). In Sodankylä and Pallas the optimal number suggested by the indices varied from 1 to 8, but for simplicity and to be able to compare sites together we chose 3.

2.3.3 Associating the snow depth clusters with snow depth measurement sensors

The Δsnow model (Winkler et al., 2021) needs daily snow depth reference measurements to be able to upscale the snow depths for the entire study area. As only a single daily snow depth sensor is available in both Pallas, we used interpolated snow depths from snow course data as reference values for the model. The snow depth measurements are conducted once a month in Sodankylä and Pallas snow courses (Fig. 1a, 1b), and during each of the drone campaigns (Fig. 2).

Snow depth measurements from snow courses were linearly interpolated to estimate snow depths between manual observations. To improve the accuracy of these estimates, the interpolated values were adjusted using daily snow depth changed recorded by the in-situ snow depth sensors (Fig. 1a, 1b). At each snow course location, the interpolated snow depth was corrected by adding the daily change observed at the representative. Unlike Pallas, where one reference sensor is available, Sodankylä has multiple ultrasonic snow depth sensors distributed across different environments, allowing more representative corrections. To account for spatial variability in snow accumulation and melt, three reference sensors were selected: one in a mire, one in a forest, and one in a forest opening (Sect. 2.2.4). Each snow course measurement point is assigned to one of these environmental categories, ensuring that the most

https://doi.org/10.5194/egusphere-2025-1297
Preprint. Discussion started: 5 May 2025

appropriate sensor was used for correction. If the corrected snow depth estimate resulted in a negative value, it was set to zero.

For the clustering model details and equations, we refer to Geissler et al. (2023). The cluster numbers are assigned so that the cluster with the highest mean snow depth gets the lowest number (cluster 1). The random forest model output $w_{ij,\,c}$ is used to calculate probabilities of snow course measurement points (s) belonging to the clusters ($w_{s,c}$) are assigned by normalizing, so that they sum to one in each cluster according to Equation 4:

$$\widehat{w_{s,c}} = \frac{w_{s,c}}{\sum_{s}(w_{s,c})} \qquad \text{(Eq. 4)}$$

The synthetic daily snow depths for each cluster $SD_c\,(t)$ are calculated by multiplying the normalized probabilities by the snow depth values of the corresponding snow course measurements and summing them for each cluster according to Equation 5:

$$SD_c\,(t) = \widehat{w_{s,c}} \times SD_s(t) \qquad \text{(Eq. 5)}$$

2.3.4 Creating daily SD and SWE maps

The synthetic snow depth (SD) maps $SD_{ij}(t)$ are generated by combining synthetic daily snow depth data ($SD_c\,(t)$) with cluster probabilities $w_{ij,c}$ and multiplying it with the time series data of that cluster ($SD_c\,(t)$) according to Equation 6:

$$SD_{ij}(t) = \sum_{c} (w_{ij,c} \times SD_c(t)) \qquad \text{(Eq. 6)}$$

The synthetic daily snow depth data for clusters was converted into SWE time series using Δsnow model (Winkler et al., 2021). The model consists of four modules, namely new snow and overburden, dry compaction, drenching or scaling modules, and each module is activated depending on the change of snow depth between time steps. The model has 7 parameters to be calibrated, where Fontrodona-Bach et al. (2023) suggested two of them to significantly related to the site-specific climate variables. These two key parameters are maximum density of a snow layer (ρmax) and new snow density ($\rho 0$). Only Sodankylä has snow measurements allowing the determination of $\rho 0$. In other sites the model was run with the values of $\rho 0$ and ρmax provided by Fontrodona-Bach et al. (2023). The rest of the 7 parameters were kept as default on Winkler et al. (2021). More information on supportive information.
The daily SWE maps $SWE_{ij}(t)$ are calculated using the synthetic snow depth data $SD_c\,(t)$ as an input for the model and then using the same protocol as for HS maps to upscale the daily SWE estimates for the entire study area using Equation 7:

$$SWE_{ij}(t) = \sum_{c} (W_{ij,c} \times SWE_c(t)) \qquad \text{(Eq. 7)}$$

3 Results

3.1 Accuracy of UAV based lidar for mapping snow depth in boreal and sub-arctic zone

At all study sites, the snow depth measured from snow courses increases until March, after which it starts to decrease due to spring melting (Table 2). Variation of snow depths increases towards the melting season and in the April campaign and the last campaign in May shows stabilization in variability as the snow has already melted from most parts.

https://doi.org/10.5194/egusphere-2025-1297
Preprint. Discussion started: 5 May 2025

Table 2. Manual snow course measurements in different campaigns and sites on winter 2023-2024.

Site	January campaign	March campaign	April campaign	May campaign
Pallas	73.8 cm; SD 4.2 cm	98.2 cm; SD 6.3 cm	95.2 cm; SD 11.6 cm	46.1 cm; SD 12.3 cm
Sodankylä	53.9 cm; SD 5.8 cm	62.2 cm; SD 9.4cm	46.3 cm; SD 19.5cm	22.4 cm; SD 6.5cm

The uncertainty of the derived DTMs were studied by comparing GCP points to the UAS DTMs (Sect. 2.2.1). The difference between UAV LiDAR snow depth maps and RTK measured GCP (Eq. 1) resulted in varying accuracy between sites and campaigns and their RMSES can be seen in Table 3. Weather conditions as well as the accuracy of RTK signal might cause differences not directly related to the UAV LiDAR.

Table 3. The RMSE of the differences between GCP plates and LiDAR UAV snow depths and the precicion and trueness of snow depth maps derived from snow depth maps in different campaigns and sites (Eq.1; Eq.2; Eq.3).

Metrics	Campaign	Sodankylä (cm)	Pallas (cm)
RMSE (Eq. 1)	January	3.1	6.8
	March	6.5	1.2
	April	5.3	3.8
	May	22.8	7.1
	June	2.4	5.1
	All	11.2	5.3
Precision (Eq. 2)	January	6.6	8.8
	March	4.5	4.7
	April	3.9	6.1
	May	20.8	6.3
	Mean	8.8	6.5
Trueness (Eq. 3)	January	2.7	3.3
	March	5.1	3.2
	April	0.9	3.3
	May	13.2	6.7
	Mean	5.3	4.1

Table 3 summarizes also the precisions of snow depth maps from standard deviations for each site calculated by Eq. (2). The precision of the snow depth maps in Sodankylä is stable during the winter campaigns, performing the best in April (4.5 cm), but has an uncertainty of 20.8 cm in May. In Pallas the precision ranges from 4.7 cm in March to 8.8 cm in January. The error propagation for mean error, meaning trueness of snow depth maps calculated by Eq. (3) are also concluded in Table 3. In Sodankylä the trueness is the best in April (0.9 cm), decreasing in May up to 13.2 cm, mostly caused by the computation of DTM with flooding of the mire areas. Pallas also has the highest trueness in the beginning of the winter with relatively stable accuracies through the winter ranging from 3.2 cm-3.3 cm in January-April and decreasing in May to 6.7 cm.

3.2 The characteristics of the snow depth clusters show similarities among sites

The characteristics of different snow depth clusters and their associated snow conditions at each site were analyzed by grouping snow course measurements and environmental data according to their respective cluster classifications.

3.2.1 Sodankylä snow depth and SWE clusters

Cluster 1 covers 21% of the total Sodankylä area, typically located in forests or pine mires (Fig. 3). It has an average canopy height of 4.6m and is located typically less than a meter away from forests (Table 4). This cluster has the

https://doi.org/10.5194/egusphere-2025-1297
Preprint. Discussion started: 5 May 2025

315 highest average modelled snow depth and SWE through the winter. According to the model, snow depth peaks at 14.3.2024 with 75 cm and SWE at 23.4.2024 with 164 mm (Table 4). The snow depth starts decreasing after the peak but increased again at the end of April due to heavy snowfall events, decreasing rapidly afterwards. From snow course measurements, the points classified to this cluster show their snow depth peak in 26.3.2024 with an average of 72.5 cm snow depth (Fig. S1, supplementary material). None of the 7 SWE measurement points of the snow course were
320 classified to this cluster (Fig. 3).

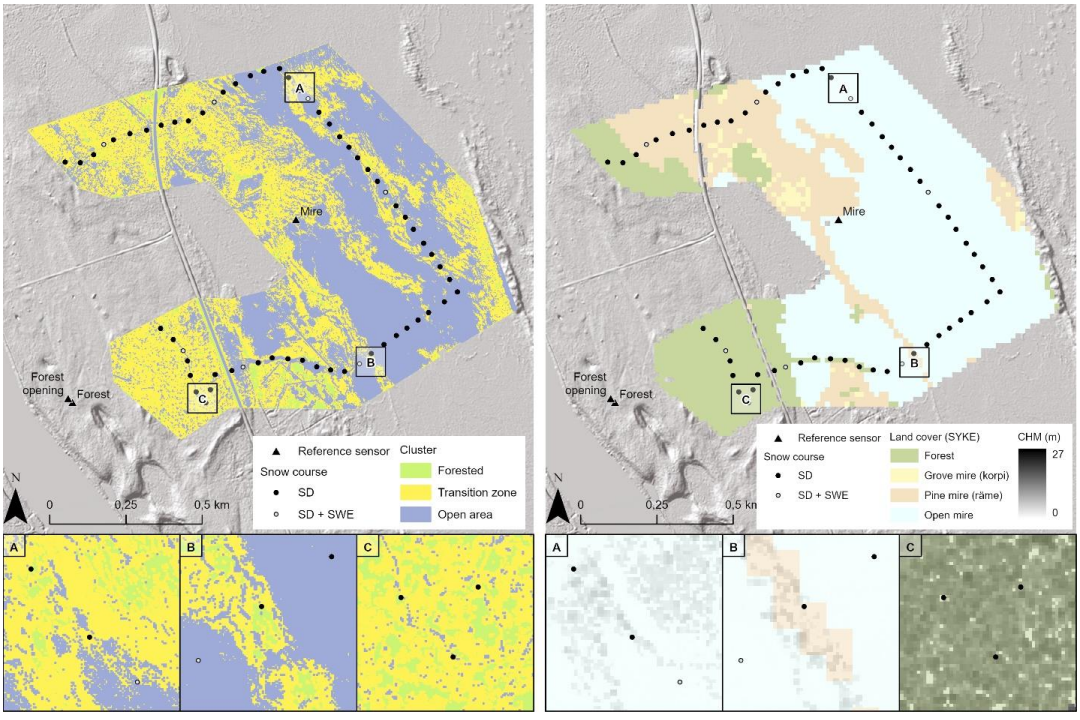

Figure 3. Sodankylä site cluster and vegetation characteristics. Bounding boxes A, B and C are examples of different cluster zones in relation to their canopy height and land cover.

325 **Table 4. Cluster characteristics in relation to the entire study area of both sites**

Site	**Sodankylä**			**Pallas**		
Cluster	**1**	**2**	**3**	**1**	**2**	**3**
Frequency %	21	45	34	32	42	26
Mineral soil (forests) %	29	25	6	78	58	55
Grove mire (korpi) %	3	2	1	2	4	2
Pine mire (räme) %	49	19	5	17	18	9
Open mire (avosuo) %	20	54	87	3	20	33
CHM (m) mean	4.6	4.7	1.8	4.3	6.2	7.5
Distance to forest (m) mean	1	3	14	1	2	7.5
Max modelled snow depth (cm)	75	70	59	111	106	103
Max modelled SWE (mm)	164	147	114	267	247	234

https://doi.org/10.5194/egusphere-2025-1297
Preprint. Discussion started: 5 May 2025

Cluster 2 is the most common, covering 45% of the total area, and is primarily located in the transition zone between forest and open areas, including forest gaps, mire edges, and forest-mire boundaries (Fig. 3). This cluster has a mean canopy height of 4.7 m and is on average 3 meters from cells classified as forests (Table 4). The modelled peak snow depth occurs 14.3.2024 (70 cm) and SWE at 23.4.2024 with 147 mm (Table 4). Snow course measurements that are classified as cluster 2 have their snow depth peaking in 15.3.2024 with an average of 67 cm, and SWE in 24.4.2024, with an average of 166 mm (Fig. S1, supplementary material).

Cluster 3 predominantly occurs in open areas with low canopy height, with 87% of the area classified as open mire. This cluster consistently exhibits the lowest snow depths and SWE values compared to the others (Fig. S1, supplementary material). The highest modelled snow depth and SWE values for cluster 3 are at the same time as for other clusters, snow depth peaking at 14.3.2024 (59 cm) and 23.4.2024 (114 mm). The snow course snow depths and SWE from cluster 3 both peak 15.3.2024 with an average snow depth of 57 cm and SWE of 138 mm.

3.2.2 Pallas snow depth and SWE clusters

In Pallas, the three clusters derived from snow depth maps also show similar characteristics to those in Sodankylä (Table 4). The most common cluster 2 covers 42% of the study area, where cluster 1 covers 32% and cluster 3 is the smallest, covering 26% of the area. The snow depth in Pallas snow course began to decrease as early as late February across all clusters (Fig. S2, supplementary material). The decline was less pronounced in points classified as cluster 1 compared to the other two clusters. However, the timing of peak SWE, marking the onset of snowmelt was later in the spring compared with snow depth and varied among the clusters.

Cluster 1 is predominantly located in the forested areas, which accounts for 78% of the cluster, while the open areas cover only 3% (Table 4). The mean canopy height is approximately 4.3m and distance to the forest cells is less than 1m, which is less than in other groups, suggesting smaller and denser forest types. Until January, modelled snow depths for cluster 1 follow similar snow depths with the other clusters, but after February they surpass those of other clusters and remain the highest until the end of the season (Fig. S2, supplementary material). Changes in the snow depths between February and March are small, with occasional fluctuations. The modelled snow depth of cluster 1 peaks at 28.3.2024 (111 cm) and the SWE peaks in 10.5.2024 with SWE of 267 mm. Snow measurements from snow course show that points classified to this cluster have their peaks in snow depth in 22.2.2024 and 25.4.2024 with both having an average snow depth of 102 cm and SWE in 25.4.2024 with 265 mm.

Cluster 2, identified as a transition zone, is typically located near forest edges, forest openings and small-scale open mire areas (Fig. 4). Forested areas cover 58% of the cluster, while open mire areas contribute 20%. The mean canopy height is approximately 6m with 2.2m distance to forest edges (Table 4). The snow depth patterns for this cluster align those of other clusters until late February, after which the snow depths in cluster 2 start to decrease. The modelled snow depth peaks in mid-March at 18.3.2024 with 106 cm, but also 17.2.2024 with 105 cm. The modelled SWE peaks later, on 28.4.204 with 247 mm and in 10.5.2024 with a SWE of 248 mm. The results are similar to the manual snow course measurements, where points classified to this cluster have their SD peak in 22.2.2024 (101 cm). However, snow course SWE peaks twice, having an average of 227 mm in 27.3.2024 and 233 mm in 25.4.2024.

Cluster 3 covers 26% of the Pallas area and is marked by a mixture of forest (55%) and open mire (33%) environments (Fig. 4). It has the greatest distance to forest cells and the tallest mean canopy height of 7.5m (Table 4). This cluster is typically found in open mires or high canopy forests. Modelled snow depths in cluster 3 are initially the highest at the start of the season but exhibit a lower rate of increase compared to the other clusters after January and remain the lowest throughout the rest of the season (Fig. S2, supplementary material). The peak modelled snow depth, 103 cm, occurs in late February 17.2.2024, after which the snow depth steadily declines. The modelled SWE peak is at the same time as for cluster 2, at 28.4.2024 (237 mm). Snow course snow depth measurements are the highest at 22.2.2024 with an average of 96 cm. SWE measurements from snow course within this cluster are limited, with only five

https://doi.org/10.5194/egusphere-2025-1297
Preprint. Discussion started: 5 May 2025

measurements taken during the melting period in late April and early May. During this period, SWE values are initially low but peak at 186 mm at 7.5.2024 (Fig. S2, supplementary material).

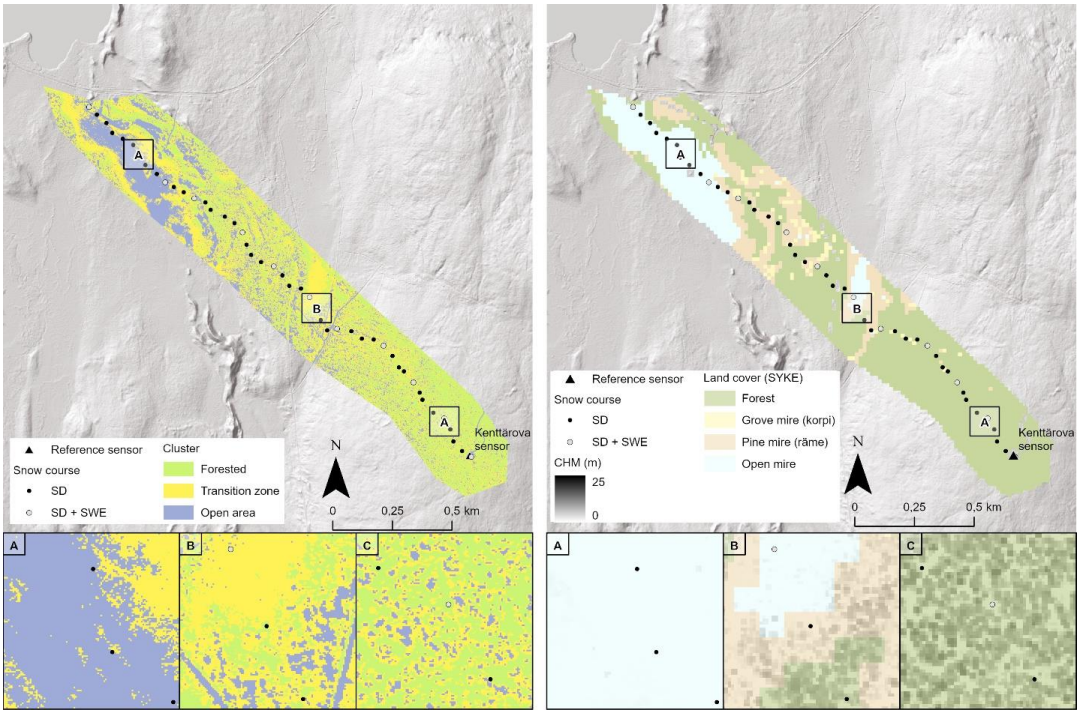

Figure 4. Pallas site cluster and vegetation characteristics. Bounding boxes A, B and C are examples of different cluster zones in relation to their vegetation.

3.2.4 UAV accuracy in comparison to clusters

To evaluate the accuracy of LiDAR UAV snow depths by cluster, snow course SD measurements were assigned to their representative cluster. When comparing the LiDAR UAV SD maps and manual snow course SD measurements, the LiDAR maps consistently underestimate the snow course measurements in both Pallas and Sodankylä (Fig. 5a, 5b). In Sodankylä, all snow course measurement campaigns show similar correspondence to the LiDAR snow depth maps and variations among clusters are similar, showing consistent agreement with snow course measurements (Fig. 5a). In Pallas the snow course measurements classified as cluster 1 correspond the best to the LiDAR snow depth maps, while the largest discrepancies are observed in cluster 3, typically located in wet mire areas (Fig. 5b). The accuracy of UAV LiDAR maps decreases towards melting season, where especially in Pallas the SD estimates are on average up to -30 cm of the snow course measurements.

https://doi.org/10.5194/egusphere-2025-1297
Preprint. Discussion started: 5 May 2025

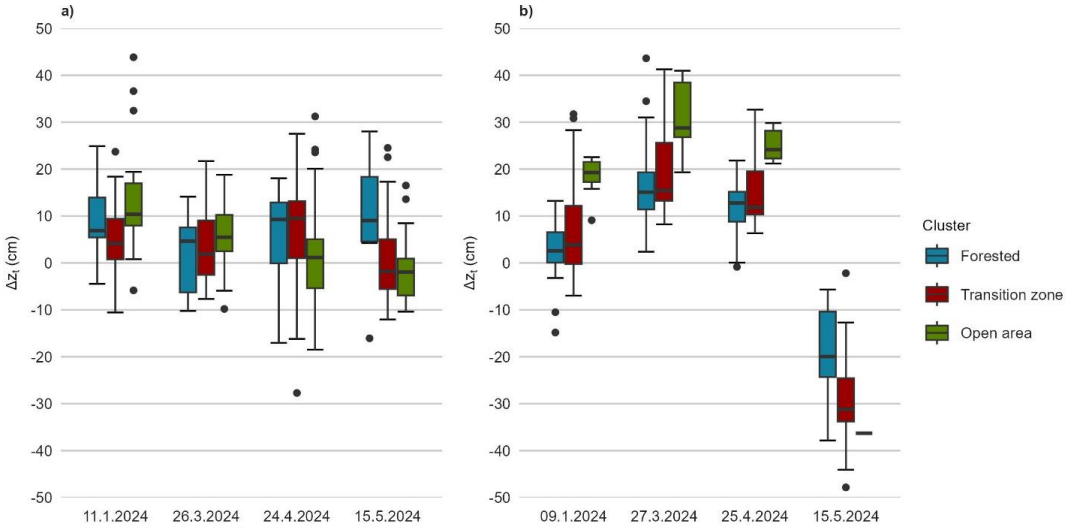

Figure 5. Difference Δz_t(cm) between the LiDAR UAV snow depths and snow course measurements by each campaign and representative cluster in (a) Sodankylä and (b) Pallas.

Snow course measurements and the UAV LiDAR snow depth for each campaign were compared with the reference snow depth sensor measurements of the study area (Fig. 1; Fig. 2) to define the overall representativeness of the measurements and clusters. In Sodankylä, all forementioned follow similar patterns; clusters have similar mean snow depth as the sensors and are within the ranges of snow course measurements (Fig. 6a), except in May, when the snow course snow depths do not match UAV LiDAR nor the sensor snow depths. The highest snow depths are in forested clustr, and reference sensor located in the forest opening. In Pallas, the UAV LiDAR snow depth maps underestimate the snow height in relation to both snow course measurements and reference snow measurement (Fig. 6b). Cluster 1 has the highest correspondence to the snow course and reference sensor compared to the areas classified as other clusters.

https://doi.org/10.5194/egusphere-2025-1297
Preprint. Discussion started: 5 May 2025

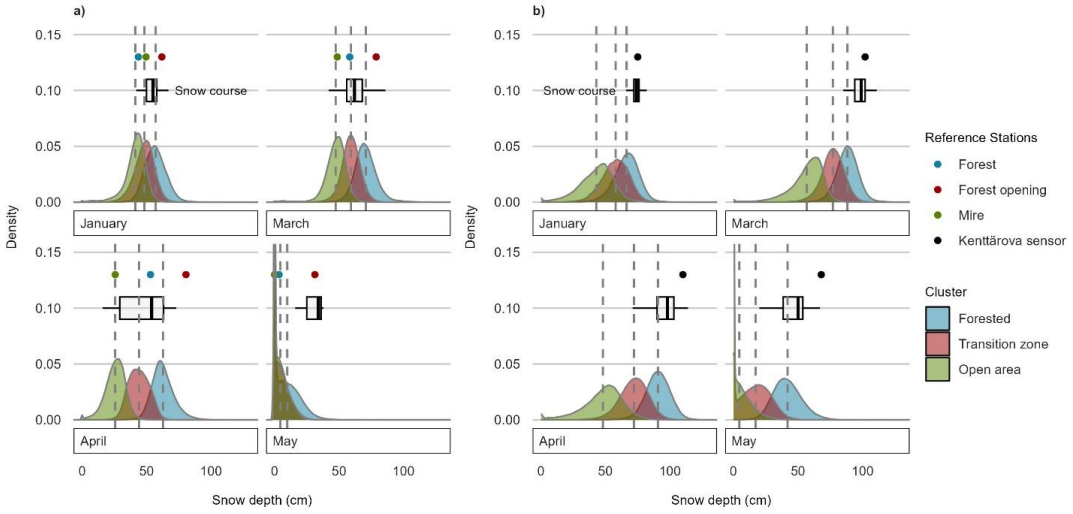

Figure 6. Reference sensor snow depths compared to UAV LiDAR snow depths by cluster in Sodankylä (a) and Pallas (b) in each campaign.

3.3 Model validation

3.3.1 Comparison of modelling results to snow course data

The model creates daily snow depth and SWE estimates for the study site. These estimates were compared to the snow course measurements and UAV LiDAR snow depth maps to estimate their accuracy (Table 5). The snow depth predictions of modelled maps have overall accuracy of 8.0 cm in Sodankylä and 5.8 cm in Pallas compared to the manual snow course measurements (Table 5). The SWE values differ from snow course measurements in Pallas with RMSE of 35.6 mm and 33.1 mm in Sodankylä during all measurements on winter 2023-2024. The predicted SWE values of Sodankylä snow course follow the observed snow course SWE values (Fig. 7a). The model tends to slightly underestimate the SWE, particularly during the late season, but the median values of measurements fall within the model's predictive range. Model performance is the highest in February, with RMSE of 12 mm (n=7). In contrast, the performance declines towards the end of the season with RMSE of 73 mm in May (n=4) as can be seen in table 7.1.

In Pallas, the modelled SWE values are typically within the range of manual SWE measurement values (Fig. 7b). The model has an overall accuracy of 32 mm (Table 5), with its best performance observed early in the season, with RMSE of 6 mm in November (n=12) and 8 mm in December (n=12) as shown in table 5. The highest error, 59 mm (n=12), occurs during the onset of the rapid snowmelt in early May. Despite this, the modelled SWE values successfully capture the peak seasonal peak in April and May, consistent with the snow course measurements.

https://doi.org/10.5194/egusphere-2025-1297
Preprint. Discussion started: 5 May 2025

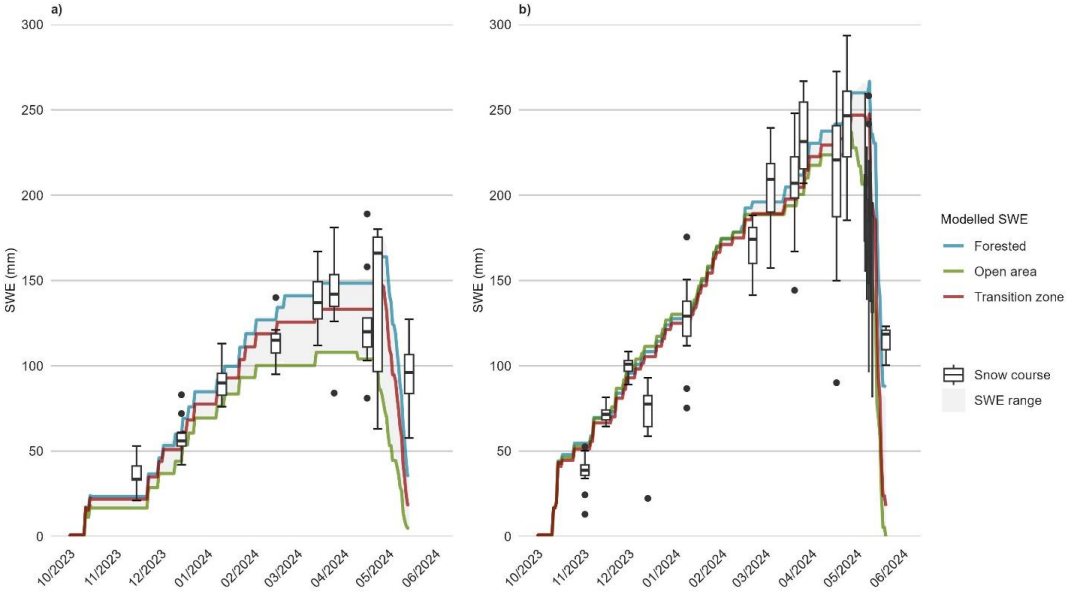

Figure 7. The modelled SWE values in comparison to the measured SWE values of the snow course in Sodankylä (a) and Pallas (b) 2023-2024.

Table 5. Sodankylä and Pallas modelled SWE RMSE

Sodankylä			**Pallas**		
Date	**RMSE SD (cm)**	**RMSE SWE (mm)**	**Date**	**RMSE SD (cm)**	**RMSE SWE (mm)**
15.11.2023	6.3 (n=62)	15 (n=7)	2.11.2023	4.5 (n =46)	18 (n=12)
15.12.2023	5.9 (n=62)	13 (n=7)	16.11.2023	4.1 (n=46)	6 (n=12)
11.1.2024	4.6 (n=62)	16 (n=7)	1.12.2023	3.9 (n=46)	8 (n=12)
16.2.2024	5.0 (n=62)	12 (n=7)	14.12.2023	3.5 (n=46)	39 (n=12)
15.3.2024	6.4 (n=62)	30 (n=7)	9.1.2024	4.1 (n=45)	25 (n=12)
26.3.2024	6.7 (n=62)	32 (n=7)	22.2.2024	4.7 (n=45)	26 (n=12)
17.4.2024	9.2 (n=60)	37 (n=6)	5.3.2024	5.2 (n=46)	26 (n=12)
24.4.2024	13.8 (n=62)	50 (n=6)	21.3.2024	5.5 (n=46)	24 (n=12)
15.5.2024	9.7 (n=62)	73 (n=4)	27.3.2024	4.8 (n=46)	34 (n=11)
Mean	**8.0 (n=555)**	**33.1 (n=58)**	18.4.2024	6.3 (n=45)	53 (n=12)
			25.4.2024	6.4 (n=45)	26 (n=12)
			4.5.2024	6.7 (n=46)	59 (n=12)
			7.5.2024	6.3 (n=46)	67 (n=12)
			15.5.2024	8.1 (n=38)	25 (n=11)
			21.5.2024	9.3 (n=46)	29 (n=3)
			Mean	**5.8 (n=677)**	**35.6 (n=169)**

https://doi.org/10.5194/egusphere-2025-1297
Preprint. Discussion started: 5 May 2025

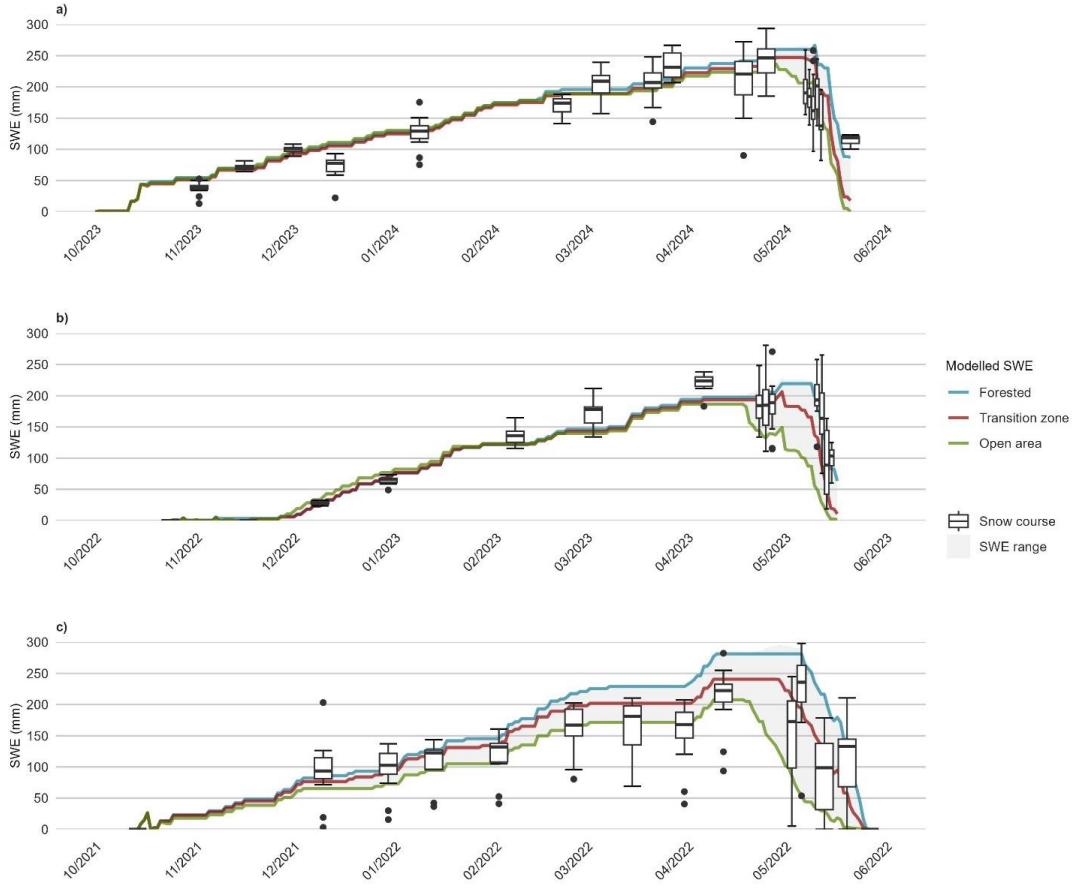

Figure 8. Modelled SWE of the previous winters (a) 2023-2024, (b) 2022-2023 and (c) 2021-2022 at Pallas in comparison to the snow course SWE measurements

The clustering and snow model (Section 2.3) provide daily maps of snow depth and SWE for each site. The defined clusters can be used for other years as well, if there is adequate snow depth data, and the spatial patterns of snow distribution are expected to be similar regardless of annual changes in snow depth and weather. Clusters defined by the snow distribution patterns of 2023-2024 were therefore used to see how well the model established based on clustering in winter 2023-2024 can reproduce previous years' snow course measurements. SWE measurements from previous years are available for Pallas starting from 2021, although the number of measurements varies across years. The results show that SWE values from winter 2022-2023 snow course are aligned with the model estimates, also capturing the peak SWE in late April (Fig. 8b). The winter of 2021–2022 exhibits the greatest variability in snowline SWE measurements, with the model overestimating SWE for most of that winter. In other winters, the model typically underestimates SWE relative to snow course measurements. Additionally, the variance in SWE values across clusters is largest during the winter of 2021–2022, reflecting greater variability in snow depth along the snow course. However, the average of the SWE from snow course on winter 2021-2022 aligns with cluster 3, and model successfully captures the SWE peak in the beginning of May 2022. The model generally captures the snow course median SWE values from the manual measurements, and the peak SWE values and its timing in previous winters.

https://doi.org/10.5194/egusphere-2025-1297
Preprint. Discussion started: 5 May 2025

3.3.2. Spatial accuracy of the model is influenced by spring floods and snow wind distribution

Figure 9 visualizes the modeled snow depths for the March campaign in Sodankylä, highlighting the influence of clustering on snow depth predictions. The modeled snow depths align with the observed snow course measurements, but the model struggles to accurately represent extreme high or low values of snow depth captured by the UAV LiDAR. The UAV LiDAR shows the spatial variability in snow depth between snow course measurement points, which are not captured during the snow course measurement survey. To be able to evaluate the model performance spatially, comparisons between modelled snow depth maps and UAV LiDAR maps were conducted for each of the campaigns. First the difference between UAV LiDAR SD map and the model SD output was derived (Fig. 10 & 11). The differences were then squared, averaged and the square root of the mean was calculated to obtain overall RMSE for the campaign and model.

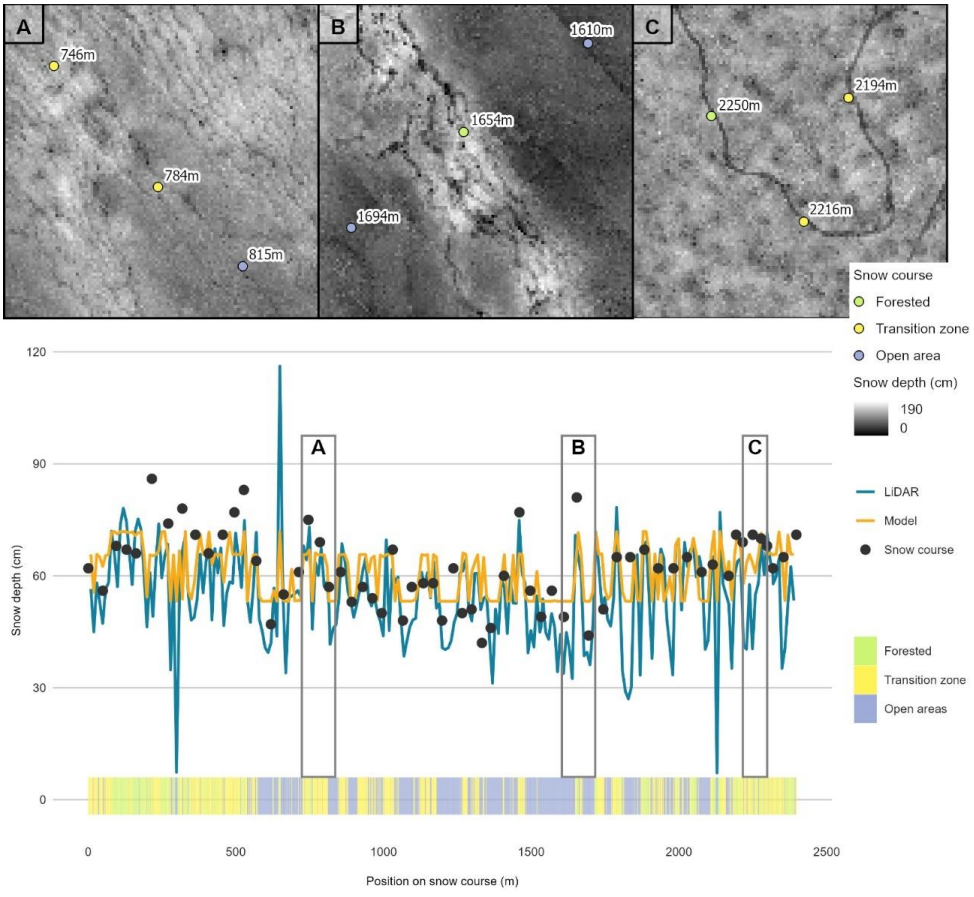

Figure 9. Transect from Sodankylä modelled snow depths, UAV LiDAR snow depths and snow course measurements and their representative clusters on 26.3.2024.

https://doi.org/10.5194/egusphere-2025-1297
Preprint. Discussion started: 5 May 2025

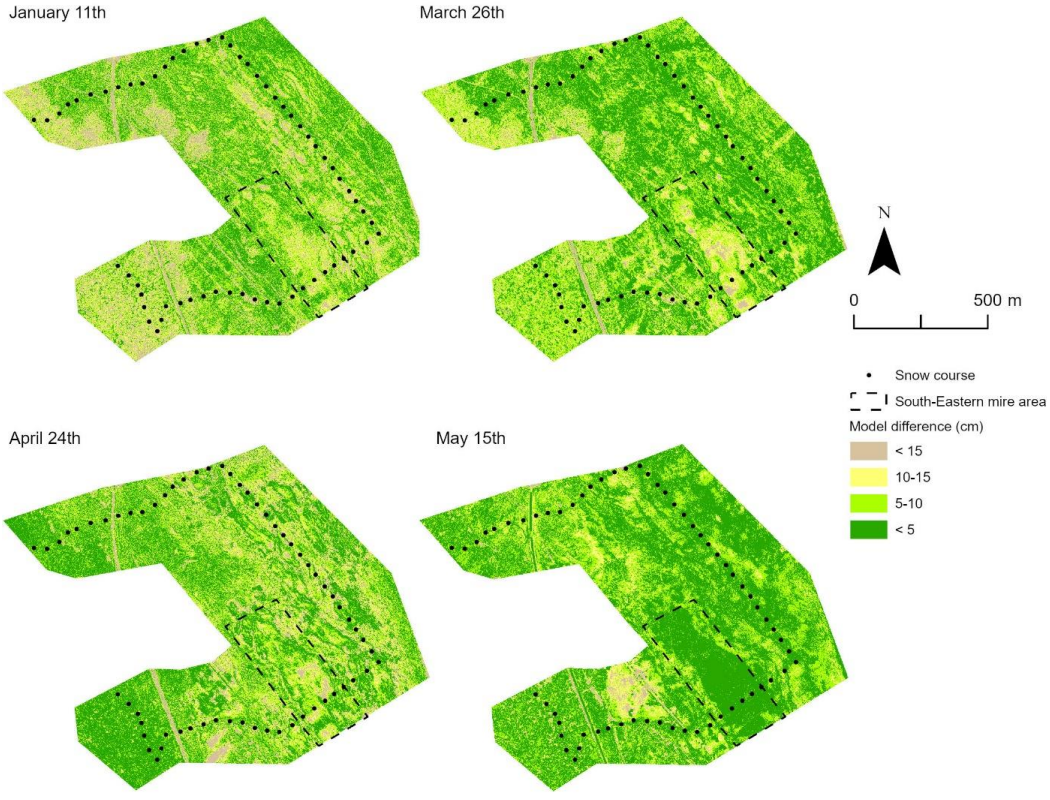

Figure 10 Sodankylä model performance from different LiDAR UAV campaigns. The values define the difference between LiDAR based snow depth maps and the modelled snow depth maps.

In Sodankylä the analysis resulted RMSEs varying from 6.2 cm to 11.0cm (January: 11.0 cm; March 8.2 cm; April; 8.8cm; May 6.2cm). The accuracy of the modeled snow depth maps is influenced more by the timing of the campaign than by the specific location (Fig. 10). For instance, in an open mire area located in the southeastern section of the snow course, the model's performance varies significantly, with difference ranging from 10–15 cm in March, decreasing to less than 5 cm in May (Fig. 10, dashed box). Similarly, in the spruce dominated forest situated in the southwestern part of the area, the highest accuracy is observed in April (difference < 5 cm), whereas in January, the model predictions exhibit a larger discrepancy, with errors ranging from 10–15 cm.

In Pallas, the model has higher inaccuracies compared to Sodankylä, with RMSEs varying from 18.7 cm to 24.7 cm (January: 22.4 cm; March 24.7 cm; April 22.7 cm; and May 18.7 cm). The model therefore performs its best at the beginning and at the end of the season. Spatially the model performs the best particularly at the southern end of the snow course, characterized by homogeneous pine and mixed forest (Fig. 11). In contrast, the model has the highest errors in the broad Lompolonjänkä mire area in the northeast, where the snow is on top of flooding mire area, and on the northern slopes of the bordering drumlins, where wind-driven snow accumulation is common. In these areas, the model estimates over 30 cm difference to the UAV LiDAR map.

https://doi.org/10.5194/egusphere-2025-1297
Preprint. Discussion started: 5 May 2025

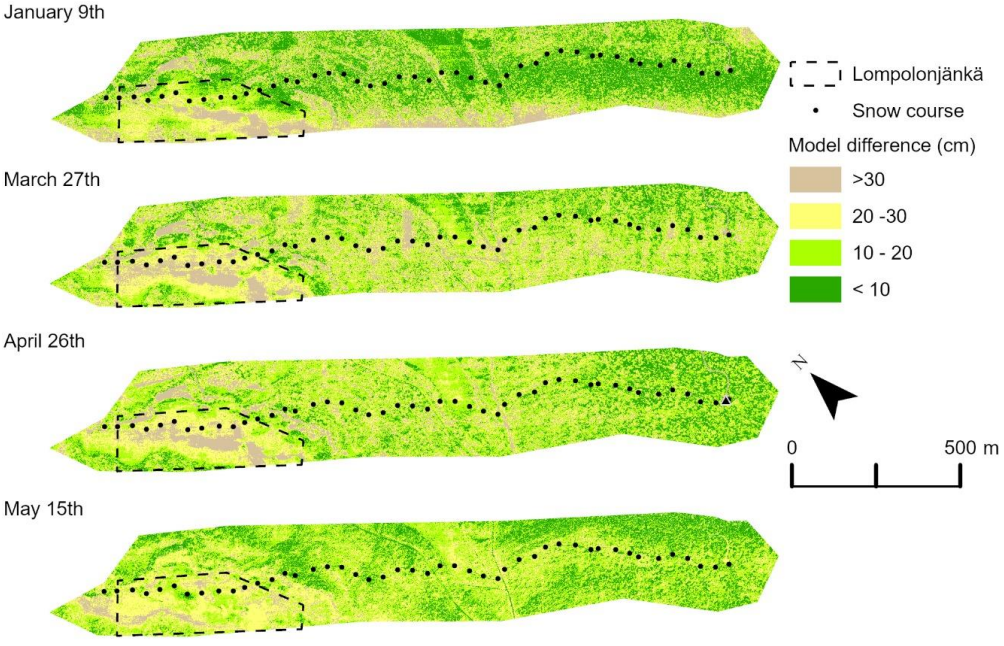

Figure 11 Pallas model performance from different LiDAR UAV campaigns. The values define the difference between UAV LiDAR snow depth maps and the model output.

4 Discussion

4.1. Snow and ice conditions impacted on UAV LiDAR accuracy

UAV LiDAR mapping showed high accuracy in all study sites and conditions, with average RMSE of UAV LiDAR DTMs being 11.2 cm and 5.3 cm for Sodankylä and Pallas, respectively. These results align with previous studies, which have reported RMSE values from snow depth maps ranging from 9 to 17 cm (Dharmadasa et al., 2022; Geissler et al., 2023; Harder et al., 2020; Jacobs et al., 2021). However, our larger uncertainty and lesser accuracy was noted in especially late melting period with flooding conditions that might be impacted by laser beams reflection from water bodies.

The trueness of the snow depth maps derived from DTM maps vary between 0.9-13 cm and typically are 4-6 cm in all sites and RMSEs of individual DTMs vary between 1 and 7 cm (excluding outlier Sodankylä May 22.1 cm). The precisions here are based on the 5 GCP measurements as suggested by Dharmadasa et al. (2022). Pallas has the most stable conditions and Sodankylä the actual lowest bias in April (0.9 cm). The accuracy of the GCP measurement itself can affect the accuracy estimates. For example, one measurement in Sodankylä May has large difference to DTM, which decreases the overall accuracy of the site. The point was not excluded from the calculations as the error can also be due to the DTM calculation errors from flooding areas. The accuracy of UAV LiDAR snow depth mapping is dependent on several factors, that can be divided into boresight errors, navigational errors, terrain- and vegetation-based errors, and post-processing-errors (Deems et al., 2013; Pilarska et al., 2016). For example, fallen tree trunks, very dense undergrowth or flooded marshes can pose challenges to point cloud classification and affect the output DTM quality (Deems et al., 2013; Evans & Hudak, 2007).

https://doi.org/10.5194/egusphere-2025-1297
Preprint. Discussion started: 5 May 2025

The best accuracy of snow depth maps (0.9 cm) of all sites and campaigns was calculated from April data from Sodankylä. Two previous days before the flight campaign on 24.4.2024 approximately 10 cm of new snow had fallen in the area, which helps to smooth the snow surface and cover previously melted or frozen areas under the snow, which could otherwise affect the laser's reflection or the accuracy of the terrain model. On contrary, the trueness of snow depth maps in all sites is the lowest in May (Table 3). Our findings highlighted increased measurement inaccuracies during that period, as most of the snow had already melted and the large areas were covered with slush and smooth water surfaces, which affects the laser beam reflection. The phenomenon can be seen in especially in Sodankylä, which has the largest, typically flooding, mire areas among sites. Up to our knowledge there is no systematical review on wet snow affecting laser beams. The results are similar with Rauhala et al. (2023), where the poorest accuracy of SfM method based DTMs were collected during the late melting period in flooding areas. This is due to the manual snow course measurements, where these flooding points are marked as having zero snow depth and DTMs still showing snow in these areas. Vegetation type, such as dense coniferous forests, are known to decrease the accuracy of different UAV methods of snow depth mapping (i.e Dharmadasa et al., 2022; Rauhala et al., 2023), as coniferous canopy prevents ground returns. If we expect the cluster 1 to present forested regions and cluster 3 to present open areas with low vegetation and compare the snow depth map accuracies to snow course measurements, we cannot distinguish similar phenomena in Sodankylä or Pallas (Fig. 5). On both sites, the best correspondence between snow course measurements and UAV LiDAR maps are in cluster 2, in forest openings. In contrast, especially in Pallas, the biggest disparities occurring in cluster 3. This can be due to snow course measurement poles lifting from the ground especially in wet areas where ground freezing and thawing move the pole during the years.

Broxton & van Leeuwen (2020) recommended the SfM method for snow depth monitoring under certain conditions, such as in gently sloping terrains and areas without dense forest cover. The UAV LiDAR method was selected over SfM method due to challenges identified, especially during the low lighting conditions and dense forest canopy cover (Rauhala et al., 2023; Revuelto et al., 2021) . With advancements in SfM camera technology, the SfM method could complement LiDAR monitoring, particularly in relatively flat regions like Sodankylä and Pallas. Nevertheless, challenges remain for both methods in large mire areas. While the SfM struggles with surface homogeneity, LiDAR faces accuracy issues in detecting bare ground under flooded, uneven and wet surfaces. Additionally, manual snow depth measurements are also less accurate due to ice and water layers on the ground.

4.2 Site characteristics explaining the different snow depth clusters

Site characteristics impacted notably to snow depth clustering in our boreal and sub-arctic sites. Especially, we noted that canopy cover, open peatlands and transition zones with wind shelter had a clear and similar influence on clustering in both sites. Additionally, we noted that the clusters have similar snow dynamics in both sites. The number of clusters has a major impact on the success of the classification, and the ability to identify specific features of each cluster depends on the quality of the clustering process.

The study employed three different categories for clustering, as initial tests demonstrated their suitability for representing different snow patterns in study areas. Equal number of clusters also provide a basis for site comparability. Our analysis resulted snow depth classification into forests with different trunk heights (cluster 1), transition zone between forests and open areas, including forest edges and gaps (cluster 2), and open areas (cluster 3) mainly peatlands. The results are consistent with those of Mazzotti et al. (2023) who noted that snow accumulation patterns can be classified in three groups based on the relationship between canopy structure and ablation rate.

In forested areas, distinguishing between clusters 1 and 2 remains challenging due to their similar site characteristics (Tables 5 & 6). Forested areas present challenges for clustering because of varying snow height and dynamics influenced by canopy cover and trunk size (L.-J. Meriö et al., 2023). Forest gaps in the coniferous forests are known to create clear and distinct variations in snow depth within the forests, and also SWE varies up to three times more in

https://doi.org/10.5194/egusphere-2025-1297
Preprint. Discussion started: 5 May 2025

unevenly distributed forests compared to evenly distributed forests (Woods et al., 2006). For this reason, forested areas contain both clusters 1 and 2 in both sites. The cluster 1 receives the most snow and has the highest SWE values, especially during the late winter (Fig. 7a; 7b). Lundquist et al. (2013) concluded that this is the typical situation in cold climates, where snow lasts longer in forests than in forest openings. In both of our sites, snowmelt starts the latest and snow cover lasts the longest in cluster 1. The forested areas in Sodankylä and Pallas are spruce dominated, where the canopy shades the ground from the sun radiation, reduces wind effects and traps snow, though also limits snowfall reaching the ground. In this cluster, we expect the snow accumulation to follow canopy structure throughout the season and the ablation to be too weak or constant to change it, as defined by Mazzotti et al. (2023).

Cluster 2 is the most common cluster on both sites (Tables 5 & 6), likely since it can be founded in both forested and open environments. While the snow depth trends across cluster 1 and cluster 2 are similar, cluster 2 experiences an earlier start of snowmelt in spring compared to forested cluster 1 (Fig. 7a; 7b). This indicates more short-wave solar radiation exposure compared to cluster 1, where SWE peaks at the end of April before the melting begins. Cluster 2 characteristics correspond to previous studies, by Koutantou et al. (2022) and Meriö et al. (2023), where canopy structure influences snow accumulation, but in ablation subsequently disrupts these patterns, resulting in earlier timing of snow loss. This phenomenon can also be seen in the modeling outputs from the previous two winters in Pallas (Fig. 8), especially in winter 2022-23, when snowmelt in cluster 2 started simultaneously with cluster 3. These characteristics are seen in both sites and support the location of the cluster 2 to be in transition zones between open and forested areas.

Open areas are subject to wind redistribution and prolonged solar exposure resulting in lower and smoother snow depth patterns, that correspond to the results of cluster 3. In cluster 3, snow depth starts decreasing notably earlier than other clusters, in February 2024, suggesting faster melting due to both higher solar radiation and flooding. In the flooding mire areas, melting waters from below also accelerate snowmelt. Both snow depth and SWE values are lower in this cluster in comparison to the other clusters, corresponding to the results from L.-J. Meriö et al. (2023). An interesting aspect of the classification is the differentiation between mires Lompolonjänkä (box A; Fig. 4) and Välisuo (box B; Fig. 4). Välisuo mire, classified to cluster 2, is more sheltered, surrounded by forests and is located at a higher altitude than the Lompolonjänkä mire, classified as cluster 3. Välisuo is drier and partly artifially drained, while Lompolonjänkä is larger drained by a small natural stream typically flooding in spring (Marttila et al., 2021).

In a recent study from Pallas site by L.-J. Meriö et al. (2023), the variations in snow depth were partially explained by canopy interception, longwave radiation emitted by trees, and wind-driven redistribution, which contributed to snow deposition along forest edges in both forested and peatland environments. The snow depth was higher within dense canopy, with the greatest accumulation observed in coniferous forest areas, followed by mixed forests, transitional forest/shrubland, and open peatlands. In both Sodankylä and Pallas the dominant winter wind direction is from the south, which leads to snow accumulation in forest canopy and their leeward side, where typically the highest snow depths are measured, corresponding to the results from Dharmadasa et al. (2023). In Pallas this results in snow accumulating particularly behind the drumlins north of the mire Lompolonjänkä (Fig. 4 Box A). This is also reflected in the accuracy of the model in these areas - the three clusters may not be sufficient to account for the particularly high snow depths of the northern sheltered slopes (Fig. 11). In comparison, snow dynamics in Sodankylä are influenced by vegetation rather than by topographical variations, as the area itself is flat with elevation differences of less than two meters. Forest structure is the main driver of snow accumulation, but shortwave radiation can disrupt these patterns, especially on south-facing slopes where there is expected more early-season ablation (Mazzotti et al., 2023). Weather further affects accumulation and ablation processes, leading to interannual variations in snow distribution, explaining why the relationship between snow distribution and canopy structure varies by location and year.

K-means clustering is widely used in many applications for partition datasets but is known to have problems associated with centroid initialization, handling outliers and dealing with various data types (Ahmed et al., 2020; Morissette & Chartier, 2013). While more clusters might be able to capture finer details, such as directional classes (Mazzotti et al.,

https://doi.org/10.5194/egusphere-2025-1297
Preprint. Discussion started: 5 May 2025

2019), the current classification to three groups corresponds to non-directional categories. These results align with previous findings that emphasize the importance of canopy structure in addition to topography and weather conditions on snow dynamics (Dharmadasa et al., 2023; Mazzotti et al., 2023). For instance, Geissler et al (2023) classified their Alpine study area into four classes, further subdividing the open class into shaded and exposed subclasses. Although using more than three clusters could potentially improve the finer scale spatial accuracy, the number of clusters is always a question of the data used and left to the user to decide, as noted also in the study of Geissler et al. (2023). Based on our observations, we conclude that the number of clusters is dependent on the landscape characteristics of the site and the purpose of the model output. If the interest is to investigate the differences between snow dynamics in different environments, we recommend increasing the cluster number to include also shaded, exposed and potentially different forest types to capture local variability (Currier & Lundquist, 2018; Fujihara et al., 2017; Mazzotti et al., 2020, 2023; Trujillo et al., 2007). However, especially in topographically homogeneous regions such as Sodankylä, less classes might be enough to represent the overall snow distribution with reasonable accuracy. The accuracy of the model output together with the homogeneous landscape supports the use of three clusters. In areas with a larger variety of terrain types, such as diverse slopes and orientations, more categories, 4 to 5, could be justified.

4.3 Lidar-based snow clustering and modeling produces SWE estimates comparable to snow surveys

The clustering derived from UAV LiDAR snow depth maps, combined with the Δsnow model, produced snow depth and SWE estimates with RMSEs of 8 cm and 33.1 mm in Sodankylä, and 5.8 cm and 35.6 mm in Pallas. The model can reproduce the onset of snowmelt and peak SWE and, after one season of drone surveys, needs only daily snow depth measurements as input. The localization of model parameters, especially ρmax and $\rho 0$, and the amount of daily snow depth reference data for the identified clusters, improved the results.

The results are consistent with a similar study by Geissler et al. (2023), where the model errors were 8 cm for snow depth and 35 mm for SWE in comparison to the manual snow measurements. Winkler et al. (2021), the creators of the presented Δsnow model, produced a SWE RMSE value for their entire validation data set of about 30.8 mm, which is consistent with other similar models and the results obtained in this study. Multilayered thermodynamic one-dimensional models for SWE estimation, such as SNOWPACK, CROCUS and SNTHERM, obtained more accurate results in the Langlois et al. (2009) study with an RMSE of 12.5-14.5 mm, but these models also require atmospheric variables that are not ubiquitously available. Studies with CROCUS also have produced SWE estimates RMSE values in the same order as this study (Vionnet et al., 2012) with an accuracy of 39.7 mm. Mortimer et al. (2020) studied the long-term gridded SWE products and compared their results to snow course measurements. None of the 9 tested products was significantly better than others, rather multiproduct combination provided the most accurate results. The lowest RMSE over Finland was 33 mm produced by ERA5. Thus, depending on the region and winter climatic conditions, there may be variability in the modelling results and our UAV results are in typical measurement estimate ranges.

The RMSE of the modelled snow depths in comparison to manual snow course measurements (Table 5) in Sodankylä are higher than in Pallas, likely due to several factors. In large mire areas, such as those found in Sodankylä, the formation of ice layer at the bottom of the snowpack may compromise the accuracy of snow course measurements (Stuefer et al., 2020). Additionally, the accuracy of snow depth maps in Sodankylä was reduced when parts of the areas were flooded in May (Table 3). Also, normalizing snow depths when generating daily estimates for clusters ensures internal consistency but reduces local variability, leading to an underestimation of extreme values. Even though the RMSE of the modeled snow depths relative to snow course measurements in Pallas is lower than in Sodankylä, the RMSEs calculated for the entire study area are higher in Pallas. Specifically, RMSE values range from 18.7 to 24.7 cm in Pallas, compared to 6.2 to 11.0 cm in Sodankylä. One contributing factor to the higher RMSE in Pallas is the accuracy of the snow course measurements (Fig. 5). The errors arise from the use of interpolated snow course data as model input. These interpolations overestimate actual snow depths in Pallas (Fig. 6), introducing a systematic bias. This overestimation of snow course measurements also partially explains the higher RMSE of the

https://doi.org/10.5194/egusphere-2025-1297
Preprint. Discussion started: 5 May 2025

Pallas SWE model compared to Sodankylä, even though the modeled snow depth estimates for snow course were more accurate (Table 5). In contrast, UAV LiDAR-derived snow depths for the entire Sodankylä region closely align with snow course measurements (Fig. 6), indicating better agreement between manual measurements and broader regional snow depth estimates in this area.

Our model can detect SWE peaks in some of the clusters (Fig. S1; S2, supplementary material). In Sodankylä, the SWE peak for cluster 2 aligns with the snow course measurements recorded at the dates between 22.4 and 24.4.2024. The model estimates SWE for cluster 3 to range between 107 and 114 mm from 14.3 to 23.4.2024 and snow course data of the cluster 3 indicates that SWE reaches its peak in mid-March before gradually decreasing until the end of April, demonstrating good agreement with the model estimates. However, while the timing of the peak is well captured, a slight discrepancy remains in its magnitude. Due to the limited number of snow course measurements classified within cluster 1, detecting meaningful correlations for this cluster was not possible. In Pallas, the model estimates SWE peaks for cluster 1 and 2 on 10.5.2024, while for cluster 33, the peak is predicted to occur earlier, on 28.4.2024. However, a slight temporal lag is observed as snow course measurements indicate that for clusters 1 and 2 the SWE peaks on 25.4.2024. For cluster 3, the discrepancy is more pronounced, with observed SWE peaking already at the end of March. The results show regional differences in SWE accumulation and melt dynamics, with the model capturing general trends but showing slight timing offsets, particularly in Pallas.

The model was validated at the Pallas site to assess its performance under different winter conditions from 2021 to 2023 from which no data was used in developing the model (Fig. 8). The results indicate that the model successfully captures both the peak SWE and its timing, despite variations in winter conditions between different years. During the 2021–2022 winter, the variance in both snow course SWE and modeled SWE is notably higher compared to the other winters. This increased variability is partly due to the fluctuating snow depths that season due to both mid-winter melt events and heavy snowfall events.

Several studies are predicting increase in mixed and liquid precipitation in winter months in Finland and, particularly in northern parts, increased solid precipitation and earlier springs (Luomaranta et al., 2019; Ruosteenoja et al., 2020). Rain-on-snow (RoS) events are expected to increase in the future for the northern Norway region during spring and summer (Mooney & Li, 2021; Pall et al., 2019), potentially leading to an increase of such events also in northern Finland. Such events increase the liquid water content of the snowpack, leading to rapid saturation and accelerated snowmelt, reducing snow depth faster than natural snowmelt processes (Yang et al., 2023). Even though Geissler et al. (2023) noticed the model's limited capacity of mapping quick changes during RoS events, the SWE estimations of this model add value to operational snow course measurements by enabling continuous monitoring of changes between monthly observations. This capability is especially valuable for capturing rapid changes during events such as snow depth variations caused by melting, snowfall, or RoS, where these dynamics can be scaled across the entire study area rather than relying on data from a single reference sensor. By integrating daily estimates from local snow depth sensors with snow course data and clusters, our approach enhances event coverage in modeling. The model's ability to capture peak snow depth and melt-out dates in real time, provided that reference snow depth sensors transmit data online, offers essential data for hydrological observation networks and improves the spatiotemporal resolution of snow course measurements.

4.4 Practical aspects and suggestions for future studies

Combining observation-based clustering with intensive field data can improve the spatiotemporal coverage of the snow course measurements and give important insights into the site-specific snow cover dynamics. Our results output is encouraging for other sites to test the approach. This study applied intensive UAV LiDAR campaigns to capture fine detailed information on snowpack variability also in forested areas, which are known to cause errors in UAV SfM methodology (Broxton & van Leeuwen, 2020) and poor lighting conditions and dense forest canopy cover (Rauhala et al., 2023; Revuelto et al., 2021). Regardless of the sensor used, the impact of winter conditions on the battery life

https://doi.org/10.5194/egusphere-2025-1297
Preprint. Discussion started: 5 May 2025

of the drone should be considered. The batteries of the DJI Matrcie 300 RTK had to be replaced up to five times during the flight campaign, especially in cold weather. Occasionally RTK coverage can also become a limiting factor in remote areas, for example in Pallas in January, due to the temporary unavailability of the VRS signal. However, especially in sparsely vegetated areas, the UAV SfM method could offer a more cost-efficient method for producing 3D data of snow dynamics and support the output of more expensive UAV LiDAR. UAV data acquisition with LiDAR or SfM can also further support the spatiotemporal resolution of remote sensing products, as their usage in local scale snow research is still limited due to spatial and temporal coverage issues (Muhuri et al., 2021; Stillinger et al., 2023; Tsang et al., 2022). As noted by Geissler et al. (2023), this method combining observations and machine learning can improve spatial representation of hyper-resolution models (Mazzotti et al., 2021) or advance refining sub-grid variability in larger-scale models (Currier & Lundquist, 2018).

Mazzotti et al. (2023) indicated that the snow distribution patterns found at a specific location may not be consistent from year to year, especially in changing weather conditions. The snow distribution patterns are site-specific due to vegetational and topographical differences, and some clusters might have different responses to different weather conditions. Especially winters with abnormal snowfall cause differences in snow extents and snow depth variability (Pflug & Lundquist, 2020). A follow-up year with different weather conditions could enhance and verify the representativeness of the clusters and provide insights into interannual variability, as local snow distribution patterns show recurrent similarities (Sturm & Wagner, 2010).

Improvements in the input data quality can enhance the accuracy of the model, but the model also seems robust, for example for Pallas site snow course measurement errors (Table 5). We would recommend a more comprehensive network of snow depth sensors that could improve daily snow depth forecasts based on snow course measurements, particularly in Pallas, where only limited data from Kenttärova snow depth sensor is available. At least one reference sensor in each land cover type, corresponding to a cluster, would improve the estimates. As fresh snow density and maximum snow density are among the most important parameters of the model (Fontrodona-Bach et al., 2023), the model parameters should be localized for each site, rather than relying on estimates based on literature. Additionally, as the greatest inaccuracies in snow course measurements at Pallas were observed in mire areas, it is important to acknowledge that these regions are prone to larger errors in both manual and UAV-based snow depth data collection. Beyond the influence of snow-forest interactions, our results also emphasize the need to study snow accumulation and melt processes in extensive peatland areas, which are particularly prevalent in the Arctic boreal zone.

5. Conclusions

This work combines emerging methods in close-range remote sensing and machine learning for high spatial and temporal resolution estimates of snow depth and snow water equivalent. The work is an important new application of such methodology in the vast, yet relatively underexplored, boreal and sub-arctic snow regimes. The study used an intensive field campaign at two well-established snow and hydrology research sites, Sodankylä and Pallas in Finnish Lapland. The different sites represent different conditions both in terms of topography and there were also significant differences in weather conditions between the different campaigns. The snow depth maps from different areas and in different winter conditions are the first from these study areas at a centimeter scale of accuracy and allow an evaluation of the method in relation to other snow depth and SWE products.

The used clustering approach together with the Δsnow model has potential for expanding the current operational snow monitoring network to different sites. The resulting SWE and snow depth maps are possible to produce in areas with snow depth sensors in different terrain types, or a regularly measured snow course with at least one snow depth sensor measuring daily. While the accuracy of the snow course measurements must be considered, the existing snow courses provide a good basis for similar approaches for local scale SWE and snow depth mapping in other boreal sites too. Even though clusters formed here are based on one winter and are site specific, we showed how they translate well to

https://doi.org/10.5194/egusphere-2025-1297
Preprint. Discussion started: 5 May 2025

different winters with different snow amounts at the sites. Founded on the well-established consistency of local-scale snow distribution between years, new technology applied in this research enables cost-effective solutions for SWE monitoring after one winter of UAV LiDAR surveys. Our work extends the previous applications of similar methods successfully to boreal taiga snow, where forest greatly complicates any snow monitoring, remote sensing and modeling.

With climate change leading to increasingly variable weather and more frequent rain-on-snow events, this methodology provides valuable tools for estimating rapid changes in snow depth and SWE at both local and catchment scales. Such spatially and temporally refined estimates of the snowpack condition are needed for catchment scale snow model validation and calibration, as well as to improve resource planning and prediction.

Acknowledgements

We gratefully acknowledge the support of Joschka Geissler with model refining and discussion. We thank Joni Koivula (UOULU), Célestin Paquet, Markku Ahponen (FMI), Anna Kontu (FMI), Aleksi Rimali (FMI), and Mirka Hatanpää (Metsähallitus) for significant help with field sampling campaigns.

The work was by funded by the European Union - NextGenerationEU CRYO-RI project (grant no. 352758) and LumiMuutos project by Maa- ja vesitekniikan tuki ry. Ala-aho was supported by the Research Council of Finland SNOMLT project (grant no. 347348). Work was supported by Digital Waters (DIWA) flagship and received funding from HYDRO-RI-Platform project and the European Union – NextGenerationEU instrument funded by the Research Council of Finland under grant number 346163. Korpelainen, Kumpula and Kuzmin was supported by Research Council of Finland funded project C-NEUT (grant no. 347862).

AI tools were used to assist in code writing and text editing.

Code and data availability

The code of the model and data used in this study with its documentation are available at https://doi.org/10.23729/fd-561771be-24b6-354b-bdd7-1b2bb6068308 (Ylönen et al., 2025) under Creative Commons Attribution 4.0 International (CC BY 4.0) license.

Supplementary material

The supplement related to this article is available online at https://doi.org/10.23729/fd-561771be-24b6-354b-bdd7-1b2bb6068308.

References

Aakala, T., Hari, P., Dengel, S., Newberry, S. L., Mizunuma, T., & Grace, J. (2014). A prominent stepwise advance of the tree line in north-east Finland. *Journal of Ecology*, *102*(6), 1582–1591. https://doi.org/https://doi.org/10.1111/1365-2745.12308

https://doi.org/10.5194/egusphere-2025-1297
Preprint. Discussion started: 5 May 2025

Adams, M. S., Bühler, Y., & Fromm, R. (2018). Multitemporal Accuracy and Precision Assessment of Unmanned Aerial System Photogrammetry for Slope-Scale Snow Depth Maps in Alpine Terrain. *Pure and Applied Geophysics*, *175*(9), 3303–3324. https://doi.org/10.1007/s00024-017-1748-y

Ahmed, M., Seraj, R., & Islam, S. M. S. (2020). The k-means Algorithm: A Comprehensive Survey and Performance Evaluation. *Electronics*, *9*(8), 1295. https://doi.org/10.3390/electronics9081295

Ala-Aho, P., Autio, A., Bhattacharjee, J., Isokangas, E., Kujala, K., Marttila, H., Menberu, M., Meriö, L.-J., Postila, H., Rauhala, A., Ronkanen, A.-K., Rossi, P. M., Saari, M., Haghighi, A. T., & Kløve, B. (2021). What conditions favor the influence of seasonally frozen ground on hydrological partitioning? A systematic review. *Environmental Research Letters*, *16*(4), 043008. https://doi.org/10.1088/1748-9326/abe82c

Bavay, M., Grünewald, T., & Lehning, M. (2013). Response of snow cover and runoff to climate change in high Alpine catchments of Eastern Switzerland. *Advances in Water Resources*, *55*, 4–16. https://doi.org/10.1016/J.ADVWATRES.2012.12.009

Beaudoin-Galaise, M., & Jutras, S. (2022). Comparison of manual snow water equivalent (SWE) measurements: seeking the reference for a true SWE value in a boreal biome. *The Cryosphere*, *16*(8), 3199–3214. https://doi.org/10.5194/tc-16-3199-2022

Berghuijs, W. R., & Hale, K. (2025). Streamflow shifts with declining snowfall. *Nature*, *638*(8052), E35–E37. https://doi.org/10.1038/s41586-024-08523-5

Bhardwaj, A., Sam, L., Bhardwaj, A., & Martín-Torres, F. J. (2016). LiDAR remote sensing of the cryosphere: Present applications and future prospects. *Remote Sensing of Environment*, *177*, 125–143. https://doi.org/10.1016/J.RSE.2016.02.031

Bouchard, B., Nadeau, D. F., & Domine, F. (2022). Comparison of snowpack structure in gaps and under the canopy in a humid boreal forest. *Hydrological Processes*, *36*(9). https://doi.org/10.1002/hyp.14681

Broxton, P. D., & van Leeuwen, W. J. D. (2020). Structure from Motion of Multi-Angle RPAS Imagery Complements Larger-Scale Airborne Lidar Data for Cost-Effective Snow Monitoring in Mountain Forests. *Remote Sensing*, *12*(14), 2311. https://doi.org/10.3390/rs12142311

Broxton, P. D., van Leeuwen, W. J. D., & Biederman, J. A. (2019). Improving Snow Water Equivalent Maps With Machine Learning of Snow Survey and Lidar Measurements. *Water Resources Research*, *55*(5), 3739–3757. https://doi.org/10.1029/2018WR024146

Busseau, B. C., Royer, A., Roy, A., Langlois, A., & Domine, F. (2017). Analysis of snow-vegetation interactions in the low Arctic-Subarctic transition zone (northeastern Canada). *Physical Geography*, *38*(2), 159–175. https://doi.org/10.1080/02723646.2017.1283477

Callaghan, T. V, Johansson, M., Brown, R. D., Groisman, P. Ya., Labba, N., Radionov, V., Bradley, R. S., Blangy, S., Bulygina, O. N., Christensen, T. R., Colman, J. E., Essery, R. L. H., Forbes, B. C., Forchhammer, M. C., Golubev, V. N., Honrath, R. E., Juday, G. P., Meshcherskaya, A. V, Phoenix, G. K., … Wood, E. F. (2011). Multiple Effects of Changes in Arctic Snow Cover. *AMBIO*, *40*(1), 32–45. https://doi.org/10.1007/s13280-011-0213-x

https://doi.org/10.5194/egusphere-2025-1297
Preprint. Discussion started: 5 May 2025

Charrad, M., Ghazzali, N., Boiteau, V., & Niknafs, A. (2014). Nbclust: An R package for determining the relevant number of clusters in a data set. *Journal of Statistical Software*, *61*(6), 1–36. https://doi.org/10.18637/jss.v061.i06

Colombo, N., Valt, M., Romano, E., Salerno, F., Godone, D., Cianfarra, P., Freppaz, M., Maugeri, M., & Guyennon, N. (2022). Long-term trend of snow water equivalent in the Italian Alps. *Journal of Hydrology*, *614*, 128532. https://doi.org/10.1016/j.jhydrol.2022.128532

Croghan, D., Ala-Aho, P., Lohila, A., Welker, J., Vuorenmaa, J., Kløve, B., Mustonen, K., Aurela, M., & Marttila, H. (2023). Coupling of Water-Carbon Interactions During Snowmelt in an Arctic Finland Catchment. *Water Resources Research*, *59*(5). https://doi.org/10.1029/2022WR032892

Currier, W. R., & Lundquist, J. D. (2018). Snow Depth Variability at the Forest Edge in Multiple Climates in the Western United States. *Water Resources Research*, *54*(11), 8756–8773. https://doi.org/10.1029/2018WR022553

Currier, W. R., Sun, N., Wigmosta, M., Cristea, N., & Lundquist, J. D. (2022). The impact of forest-controlled snow variability on late-season streamflow varies by climatic region and forest structure. *Hydrological Processes*, *36*(6). https://doi.org/10.1002/hyp.14614

Deems, J. S., Painter, T. H., & Finnegan, D. C. (2013). Lidar measurement of snow depth: a review. *Journal of Glaciology*, *59*(215), 467–479. https://doi.org/10.3189/2013JoG12J154

Dharmadasa, V., Kinnard, C., & Baraër, M. (2022). An Accuracy Assessment of Snow Depth Measurements in Agro-Forested Environments by UAV Lidar. *Remote Sensing*, *14*(7), 1649. https://doi.org/10.3390/rs14071649

Dharmadasa, V., Kinnard, C., & Baraër, M. (2023). Topographic and vegetation controls of the spatial distribution of snow depth in agro-forested environments by UAV lidar. *The Cryosphere*, *17*(3), 1225–1246. https://doi.org/10.5194/tc-17-1225-2023

Engelhardt, M., Schuler, T. V, & Andreassen, L. M. (2014). Contribution of snow and glacier melt to discharge for highly glacierised catchments in Norway. *Hydrology and Earth System Sciences*, *18*(2), 511–523. https://doi.org/10.5194/hess-18-511-2014

Evans, J. S., & Hudak, A. T. (2007). A Multiscale Curvature Algorithm for Classifying Discrete Return LiDAR in Forested Environments. *IEEE Transactions on Geoscience and Remote Sensing*, *45*(4), 1029–1038. https://doi.org/10.1109/TGRS.2006.890412

Faquseh, H., & Grossi, G. (2024). Trend analysis of precipitation, temperature and snow water equivalent in Lombardy region, northern Italy. *Sustainable Water Resources Management*, *10*(1), 18. https://doi.org/10.1007/s40899-023-00992-2

Fontrodona-Bach, A., Schaefli, B., Woods, R., Teuling, A. J., & Larsen, J. R. (2023). NH-SWE: Northern Hemisphere Snow Water Equivalent dataset based on in situ snow depth time series. *Earth System Science Data*, *15*(6), 2577–2599. https://doi.org/10.5194/essd-15-2577-2023

Franke, A. K., Bräuning, A., Timonen, M., & Rautio, P. (2017). Growth response of Scots pines in polar-alpine tree-line to a warming climate. *Forest Ecology and Management*, *399*, 94–107. https://doi.org/10.1016/J.FORECO.2017.05.027

https://doi.org/10.5194/egusphere-2025-1297
Preprint. Discussion started: 5 May 2025

Fujihara, Y., Takase, K., Chono, S., Ichion, E., Ogura, A., & Tanaka, K. (2017). Influence of topography and forest characteristics on snow distributions in a forested catchment. *Journal of Hydrology*, *546*, 289–298. https://doi.org/10.1016/j.jhydrol.2017.01.021

Geissler, J., Rathmann, L., & Weiler, M. (2023). Combining Daily Sensor Observations and Spatial LiDAR Data for Mapping Snow Water Equivalent in a Sub-Alpine Forest. *Water Resources Research*, *59*(9), e2023WR034460. https://doi.org/https://doi.org/10.1029/2023WR034460

Gottlieb, A. R., & Mankin, J. S. (2024). Evidence of human influence on Northern Hemisphere snow loss. *Nature*, *625*(7994), 293–300. https://doi.org/10.1038/s41586-023-06794-y

Grace, J., Berningen, F., & Nagy, L. (2002). Impacts of Climate Change on the Tree Line. *Annals of Botany*, *90*(4), 537–544. https://doi.org/10.1093/aob/mcf222

Harder, P., Pomeroy, J. W., & Helgason, W. D. (2020). Improving sub-canopy snow depth mapping with unmanned aerial vehicles: lidar versus structure-from-motion techniques. *The Cryosphere*, *14*(6), 1919–1935. https://doi.org/10.5194/tc-14-1919-2020

Hartigan, J. A., & Wong, M. A. (1979). Algorithm AS 136: A K-Means Clustering Algorithm. *Applied Statistics*, *28*(1), 100. https://doi.org/10.2307/2346830

Jacobs, J. M., Hunsaker, A. G., Sullivan, F. B., Palace, M., Burakowski, E. A., Herrick, C., & Cho, E. (2021). Snow depth mapping with unpiloted aerial system lidar observations: a case study in Durham, New Hampshire, United States. *The Cryosphere*, *15*(3), 1485–1500. https://doi.org/10.5194/tc-15-1485-2021

Jan, A., & Painter, S. L. (2020). Permafrost thermal conditions are sensitive to shifts in snow timing. *Environmental Research Letters*, *15*(8), 84026. https://doi.org/10.1088/1748-9326/ab8ec4

King, F., Erler, A. R., Frey, S. K., & Fletcher, C. G. (2020). Application of machine learning techniques for regional bias correction of snow water equivalent estimates in Ontario, Canada. *Hydrology and Earth System Sciences*, *24*(10), 4887–4902. https://doi.org/10.5194/hess-24-4887-2020

Koutantou, K., Mazzotti, G., Brunner, P., Webster, C., & Jonas, T. (2022). Exploring snow distribution dynamics in steep forested slopes with UAV-borne LiDAR. *Cold Regions Science and Technology*, *200*, 103587. https://doi.org/10.1016/j.coldregions.2022.103587

Kunkel, K. E., Robinson, D. A., Champion, S., Yin, X., Estilow, T., & Frankson, R. M. (2016). Trends and Extremes in Northern Hemisphere Snow Characteristics. *Current Climate Change Reports*, *2*(2), 65–73. https://doi.org/10.1007/s40641-016-0036-8

Kuusisto, E. (1984). Snow accumulation and snowmelt in Finland. In *Publications of the water research institute* (55th ed.). National Board of Waters.

Langlois, A., Kohn, J., Royer, A., Cliche, P., Brucker, L., Picard, G., Fily, M., Derksen, C., & Willemet, J. M. (2009). Simulation of Snow Water Equivalent (SWE) Using Thermodynamic Snow Models in Québec, Canada. *Journal of Hydrometeorology*, *10*(6), 1447–1463. https://doi.org/10.1175/2009JHM1154.1

Li, Q., Ma, M., Wu, X., & Yang, H. (2018). Snow Cover and Vegetation-Induced Decrease in Global Albedo From 2002 to 2016. *Journal of Geophysical Research: Atmospheres*, *123*(1), 124–138. https://doi.org/10.1002/2017JD027010

https://doi.org/10.5194/egusphere-2025-1297
Preprint. Discussion started: 5 May 2025

Lundquist, J. D., Dickerson-Lange, S. E., Lutz, J. A., & Cristea, N. C. (2013). Lower forest density enhances snow retention in regions with warmer winters: A global framework developed from plot-scale observations and modeling. *Water Resources Research*, *49*(10), 6356–6370. https://doi.org/https://doi.org/10.1002/wrcr.20504

Luomaranta, A., Aalto, J., & Jylhä, K. (2019). Snow cover trends in Finland over 1961–2014 based on gridded snow depth observations. *International Journal of Climatology*, *39*(7), 3147–3159. https://doi.org/https://doi.org/10.1002/joc.6007

Maier, K., Nascetti, A., van Pelt, W., & Rosqvist, G. (2022). Direct photogrammetry with multispectral imagery for UAV-based snow depth estimation. *ISPRS Journal of Photogrammetry and Remote Sensing*, *186*, 1–18. https://doi.org/10.1016/J.ISPRSJPRS.2022.01.020

Malek, S. A., Bales, R. C., & Glaser, S. D. (2020). Estimation of Daily Spatial Snow Water Equivalent from Historical Snow Maps and Limited In-Situ Measurements. *Hydrology*, *7*(3), 46. https://doi.org/10.3390/hydrology7030046

Marttila, H., Lohila, A., Ala-Aho, P., Noor, K., Welker, J. M., Croghan, D., Mustonen, K., Meriö, L., Autio, A., Muhic, F., Bailey, H., Aurela, M., Vuorenmaa, J., Penttilä, T., Hyöky, V., Klein, E., Kuzmin, A., Korpelainen, P., Kumpula, T., … Kløve, B. (2021). Subarctic catchment water storage and carbon cycling – Leading the way for future studies using integrated datasets at Pallas, Finland. *Hydrological Processes*, *35*(9). https://doi.org/10.1002/hyp.14350

Matiu, M., Crespi, A., Bertoldi, G., Carmagnola, C. M., Marty, C., Morin, S., Schöner, W., Cat Berro, D., Chiogna, G., De Gregorio, L., Kotlarski, S., Majone, B., Resch, G., Terzago, S., Valt, M., Beozzo, W., Cianfarra, P., Gouttevin, I., Marcolini, G., … Weilguni, V. (2021). Observed snow depth trends in the European Alps: 1971 to 2019. *The Cryosphere*, *15*(3), 1343–1382. https://doi.org/10.5194/tc-15-1343-2021

Matti, B., Dahlke, H., Dieppois, B., Lawler, D., & Lyon, S. (2017). Flood seasonality across Scandinavia – Evidence of a shifting hydrograph? *Hydrological Processes*, *31*. https://doi.org/10.1002/hyp.11365

Mazzotti, G., Currier, W. R., Deems, J. S., Pflug, J. M., Lundquist, J. D., & Jonas, T. (2019). Revisiting Snow Cover Variability and Canopy Structure Within Forest Stands: Insights From Airborne Lidar Data. *Water Resources Research*, *55*(7), 6198–6216. https://doi.org/https://doi.org/10.1029/2019WR024898

Mazzotti, G., Essery, R., Moeser, C. D., & Jonas, T. (2020). Resolving Small-Scale Forest Snow Patterns Using an Energy Balance Snow Model With a One-Layer Canopy. *Water Resources Research*, *56*(1). https://doi.org/10.1029/2019WR026129

Mazzotti, G., Webster, C., Essery, R., & Jonas, T. (2021). Increasing the Physical Representation of Forest-Snow Processes in Coarse-Resolution Models: Lessons Learned From Upscaling Hyper-Resolution Simulations. *Water Resources Research*, *57*(5), e2020WR029064. https://doi.org/https://doi.org/10.1029/2020WR029064

Mazzotti, G., Webster, C., Quéno, L., Cluzet, B., & Jonas, T. (2023). Canopy structure, topography, and weather are equally important drivers of small-scale snow cover dynamics in sub-alpine forests. *Hydrology and Earth System Sciences*, *27*(11), 2099–2121. https://doi.org/10.5194/hess-27-2099-2023

https://doi.org/10.5194/egusphere-2025-1297
Preprint. Discussion started: 5 May 2025

Meloche, J., Langlois, A., Rutter, N., McLennan, D., Royer, A., Billecocq, P., & Ponomarenko, S. (2022). High-resolution snow depth prediction using Random Forest algorithm with topographic parameters: A case study in the Greiner watershed, Nunavut. *Hydrological Processes*, *36*(3). https://doi.org/10.1002/hyp.14546

Meriö, L., Ala-aho, P., Linjama, J., Hjort, J., Kløve, B., & Marttila, H. (2019). Snow to Precipitation Ratio Controls Catchment Storage and Summer Flows in Boreal Headwater Catchments. *Water Resources Research*, *55*(5), 4096–4109. https://doi.org/10.1029/2018WR023031

Meriö, L.-J., Rauhala, A., Ala-aho, P., Kuzmin, A., Korpelainen, P., Kumpula, T., Kløve, B., & Marttila, H. (2023). Measuring the spatiotemporal variability in snow depth in subarctic environments using UASs – Part 2: Snow processes and snow–canopy interactions. *The Cryosphere*, *17*(10), 4363–4380. https://doi.org/10.5194/tc-17-4363-2023

Mooney, P. A., & Li, L. (2021). Near future changes to rain-on-snow events in Norway. *Environmental Research Letters*, *16*(6), 064039. https://doi.org/10.1088/1748-9326/abfdeb

Morissette, L., & Chartier, S. (2013). The k-means clustering technique: General considerations and implementation in Mathematica. *Tutorials in Quantitative Methods for Psychology*, *9*(1), 15–24. https://doi.org/10.20982/tqmp.09.1.p015

Mortimer, C., Mudryk, L., Derksen, C., Luojus, K., Brown, R., Kelly, R., & Tedesco, M. (2020). Evaluation of long-term Northern Hemisphere snow water equivalent products. *The Cryosphere*, *14*(5), 1579–1594. https://doi.org/10.5194/tc-14-1579-2020

Mudryk, L. R., Kushner, P. J., Derksen, C., & Thackeray, C. (2017). Snow cover response to temperature in observational and climate model ensembles. *Geophysical Research Letters*, *44*(2), 919–926. https://doi.org/https://doi.org/10.1002/2016GL071789

Mudryk, L., Santolaria-Ot\'{\i}n, M., Krinner, G., Ménégoz, M., Derksen, C., Brutel-Vuilmet, C., Brady, M., & Essery, R. (2020). Historical Northern Hemisphere snow cover trends and projected changes in the CMIP6 multi-model ensemble. *The Cryosphere*, *14*(7), 2495–2514. https://doi.org/10.5194/tc-14-2495-2020

Muhic, F., Ala-Aho, P., Noor, K., Welker, J. M., Klöve, B., & Marttila, H. (2023). Flushing or mixing? Stable water isotopes reveal differences in arctic forest and peatland soil water seasonality. *Hydrological Processes*, *37*(1). https://doi.org/10.1002/hyp.14811

Muhuri, A., Gascoin, S., Menzel, L., Kostadinov, T. S., Harpold, A. A., Sanmiguel-Vallelado, A., & Lopez-Moreno, J. I. (2021). Performance Assessment of Optical Satellite-Based Operational Snow Cover Monitoring Algorithms in Forested Landscapes. *IEEE Journal of Selected Topics in Applied Earth Observations and Remote Sensing*, *14*, 7159–7178. https://doi.org/10.1109/JSTARS.2021.3089655

Mustonen, S. (1965). Ilmasto- ja maastotekijöiden vaikutuksesta lumen vesiarvoon ja roudan syvyyteen. *Acta Forestalia Fennica*, *79*(1). https://doi.org/10.14214/aff.7159

Niedzielski, T., Spallek, W., & Witek-Kasprzak, M. (2018). Automated Snow Extent Mapping Based on Orthophoto Images from Unmanned Aerial Vehicles. *Pure and Applied Geophysics*, *175*(9), 3285–3302. https://doi.org/10.1007/s00024-018-1843-8

https://doi.org/10.5194/egusphere-2025-1297
Preprint. Discussion started: 5 May 2025

Nolan, M., Larsen, C., & Sturm, M. (2015). Mapping snow depth from manned aircraft on landscape scales at centimeter resolution using structure-from-motion photogrammetry. *The Cryosphere*, *9*(4), 1445–1463. https://doi.org/10.5194/tc-9-1445-2015

Okkonen, J., Ala-Aho, P., Hänninen, P., Hayashi, M., Sutinen, R., & Liwata, P. (2017). Multi-year simulation and model calibration of soil moisture and temperature profiles in till soil. *European Journal of Soil Science*, *68*(6), 829–839. https://doi.org/https://doi.org/10.1111/ejss.12489

Pall, P., Tallaksen, L. M., & Stordal, F. (2019). A Climatology of Rain-on-Snow Events for Norway. *Journal of Climate*, *32*(20), 6995–7016. https://doi.org/10.1175/JCLI-D-18-0529.1

Pflug, J. M., & Lundquist, J. D. (2020). Inferring Distributed Snow Depth by Leveraging Snow Pattern Repeatability: Investigation Using 47 Lidar Observations in the Tuolumne Watershed, Sierra Nevada, California. *Water Resources Research*, *56*(9), e2020WR027243. https://doi.org/https://doi.org/10.1029/2020WR027243

Pilarska, M., Ostrowski, W., Bakuła, K., Górski, K., & Kurczyński, Z. (2016). The potential of light laser scanners developed for unmanned aerial vehicles – the review and accuracy. *The International Archives of the Photogrammetry, Remote Sensing and Spatial Information Sciences*, *XLII-2/W2*, 87–95. https://doi.org/10.5194/isprs-archives-XLII-2-W2-87-2016

R Core Team. (2023). *R : A language and environment for statistical computing*. . R Foundation for Statistical Computing. https://www.R-project.org/

Räisänen, J. (2023). Changes in March mean snow water equivalent since the mid-20th century and the contributing factors in reanalyses and CMIP6 climate models. *The Cryosphere*, *17*(5), 1913–1934. https://doi.org/10.5194/tc-17-1913-2023

Rauhala, A., Meriö, L.-J., Kuzmin, A., Korpelainen, P., Ala-aho, P., Kumpula, T., Kløve, B., & Marttila, H. (2023). Measuring the spatiotemporal variability in snow depth in subarctic environments using UASs – Part 1: Measurements, processing, and accuracy assessment. *The Cryosphere*, *17*(10), 4343–4362. https://doi.org/10.5194/tc-17-4343-2023

Revuelto, J., Alonso-González, E., & López-Moreno, J. I. (2020). Generation of daily high-spatial resolution snow depth maps from in-situ measurement and time-lapse photographs. *Cuadernos de Investigación Geográfica*, *46*(1), 59–79. https://doi.org/10.18172/cig.3801

Revuelto, J., López-Moreno, J. I., & Alonso-González, E. (2021). Light and Shadow in Mapping Alpine Snowpack With Unmanned Aerial Vehicles in the Absence of Ground Control Points. *Water Resources Research*, *57*(6). https://doi.org/10.1029/2020WR028980

Rittger, K., Raleigh, M. S., Dozier, J., Hill, A. F., Lutz, J. A., & Painter, T. H. (2020). Canopy Adjustment and Improved Cloud Detection for Remotely Sensed Snow Cover Mapping. *Water Resources Research*, *56*(6). https://doi.org/10.1029/2019WR024914

Rogers, S. R., Manning, I., & Livingstone, W. (2020). Comparing the Spatial Accuracy of Digital Surface Models from Four Unoccupied Aerial Systems: Photogrammetry Versus LiDAR. *Remote Sensing*, *12*(17), 2806. https://doi.org/10.3390/rs12172806

https://doi.org/10.5194/egusphere-2025-1297
Preprint. Discussion started: 5 May 2025

Ropars, P., & Boudreau, S. (2012). Shrub expansion at the forest–tundra ecotone: spatial heterogeneity linked to local topography. *Environmental Research Letters*, *7*(1), 015501. https://doi.org/10.1088/1748-9326/7/1/015501

Roussel, J.-R. (2024). *lasR: Fast and Pipeable Airborne LiDAR Data Tools* (0.13.0).

Roussel, J.-R., Auty, D., Coops, N. C., Tompalski, P., Goodbody, T. R. H., Meador, A. S., Bourdon, J.-F., de Boissieu, F., & Achim, A. (2020). lidR: An R package for analysis of Airborne Laser Scanning (ALS) data. *Remote Sensing of Environment*, *251*, 112061. https://doi.org/10.1016/j.rse.2020.112061

Ruosteenoja, K., Markkanen, T., & Räisänen, J. (2020). Thermal seasons in northern Europe in projected future climate. *International Journal of Climatology*, *40*(10), 4444–4462. https://doi.org/10.1002/joc.6466

Stillinger, T., Rittger, K., Raleigh, M. S., Michell, A., Davis, R. E., & Bair, E. H. (2023). Landsat, MODIS, and VIIRS snow cover mapping algorithm performance as validated by airborne lidar datasets. *The Cryosphere*, *17*(2), 567–590. https://doi.org/10.5194/tc-17-567-2023

Stuefer, S. L., Kane, D. L., & Dean, K. M. (2020). Snow Water Equivalent Measurements in Remote Arctic Alaska Watersheds. *Water Resources Research*, *56*(4). https://doi.org/10.1029/2019WR025621

Sturm, M., & Wagner, A. M. (2010). Using repeated patterns in snow distribution modeling: An Arctic example. *Water Resources Research*, *46*(12). https://doi.org/10.1029/2010WR009434

The Finnish meteorological institute. (2025). *Säähavaintojen vuorokausi- ja kuukausiarvot*. Https://Www.Ilmatieteenlaitos.Fi/Avoin-Data-Saahavaintojen-Vrk-Ja-Kk-Arvot.

Thiebault, K., & Young, S. (2020). Snow cover change and its relationship with land surface temperature and vegetation in northeastern North America from 2000 to 2017. *International Journal of Remote Sensing*, *41*(21), 8453–8474. https://doi.org/10.1080/01431161.2020.1779379

Trujillo, E., Ramírez, J. A., & Elder, K. J. (2007). Topographic, meteorologic, and canopy controls on the scaling characteristics of the spatial distribution of snow depth fields. *Water Resources Research*, *43*(7). https://doi.org/10.1029/2006WR005317

Tsang, L., Durand, M., Derksen, C., Barros, A. P., Kang, D.-H., Lievens, H., Marshall, H.-P., Zhu, J., Johnson, J., King, J., Lemmetyinen, J., Sandells, M., Rutter, N., Siqueira, P., Nolin, A., Osmanoglu, B., Vuyovich, C., Kim, E., Taylor, D., … Xu, X. (2022). Review article: Global monitoring of snow water equivalent using high-frequency radar remote sensing. *The Cryosphere*, *16*(9), 3531–3573. https://doi.org/10.5194/tc-16-3531-2022

Vafakhah, M., Nasiri Khiavi, A., Janizadeh, S., & Ganjkhanlo, H. (2022). Evaluating different machine learning algorithms for snow water equivalent prediction. *Earth Science Informatics*, *15*(4), 2431–2445. https://doi.org/10.1007/s12145-022-00846-z

Vionnet, V., Brun, E., Morin, S., Boone, A., Faroux, S., Le Moigne, P., Martin, E., & Willemet, J.-M. (2012). The detailed snowpack scheme Crocus and its implementation in SURFEX v7.2. *Geoscientific Model Development*, *5*(3), 773–791. https://doi.org/10.5194/gmd-5-773-2012

Wang, R., Kumar, M., & Link, T. E. (2016). Potential trends in snowmelt-generated peak streamflows in a warming climate. *Geophysical Research Letters*, *43*(10), 5052–5059. https://doi.org/https://doi.org/10.1002/2016GL068935

https://doi.org/10.5194/egusphere-2025-1297
Preprint. Discussion started: 5 May 2025

Winkler, M., Schellander, H., & Gruber, S. (2021). Snow water equivalents exclusively from snow depths and their temporal changes: the Δsnow model. *Hydrology and Earth System Sciences*, *25*(3), 1165–1187. https://doi.org/10.5194/hess-25-1165-2021

Woods, S. W., Ahl, R., Sappington, J., & McCaughey, W. (2006). Snow accumulation in thinned lodgepole pine stands, Montana, USA. *Forest Ecology and Management*, *235*(1–3), 202–211. https://doi.org/10.1016/j.foreco.2006.08.013

Yang, Z., Chen, R., Liu, Y., Zhao, Y., Liu, Z., & Liu, J. (2023). The impact of rain-on-snow events on the snowmelt process: A field study. *Hydrological Processes*, *37*(11). https://doi.org/10.1002/hyp.15019

Zhang, J., Pohjola, V. A., Pettersson, R., Norell, B., Marchand, W.-D., Clemenzi, I., & Gustafsson, D. (2021). Improving the snowpack monitoring in the mountainous areas of Sweden from space: a machine learning approach. *Environmental Research Letters*, *16*(8), 84007. https://doi.org/10.1088/1748-9326/abfe8d

Zhang, Y., & Ma, N. (2018). Spatiotemporal variability of snow cover and snow water equivalent in the last three decades over Eurasia. *Journal of Hydrology*, *559*, 238–251. https://doi.org/10.1016/j.jhydrol.2018.02.031